Alcohol reverses the effects of *KCNJ6* (GIRK2) noncoding variants on excitability of human glutamatergic neurons

Running title: Alcohol reverses effects of *KCNJ6* SNPs on neurons

Dina Popova[1], Isabel Gameiro-Ros[2], Mark M. Youssef[3], Petronio Zalamea[1], Ayeshia D. Morris[4], Iya Prytkova[2], Azadeh Jadali[3], Kelvin Y. Kwan[3], Chella Kamarajan[5], Jessica E. Salvatore[6], Xiaoling Xuei[7], David B. Chorlian[5], Bernice Porjesz[5], Samuel Kuperman[8], Danielle M. Dick[9], Alison Goate[10], Howard J. Edenberg[11], Jay A. Tischfield[1], Zhiping P. Pang[1,12], Paul A. Slesinger[2] and Ronald P. Hart[1,3,*]

Affiliations:

[1]Human Genetics Institute, Rutgers University, Piscataway, NJ 08854
[2]Nash Family Department of Neuroscience, Icahn School of Medicine at Mount Sinai, New York, NY 10029
[3]Department of Cell Biology & Neuroscience, Rutgers University, Piscataway, NJ 08854
[4]Joint Program in Toxicology, Rutgers University, Piscataway, NJ 08854
[5]Dept. of Psychiatry & Behavioral Sciences, SUNY Downstate Health Sciences University, Brooklyn, NY 11203
[6]Department of Psychiatry, Rutgers Robert Wood Johnson Medical School, Rutgers University, Piscataway, NJ 08854
[7]Department of Medical and Molecular Genetics, Indiana University School of Medicine, Indianapolis, IN 46202
[8]Department of Psychiatry, University of Iowa Carver College of Medicine, Iowa City, IA 52242
[9]Rutgers Addiction Research Center, Robert Wood Johnson Medical School, Rutgers University, Piscataway, NJ 08854
[10]Department of Genetics & Genomic Sciences, Icahn School of Medicine at Mount Sinai, New York, NY 10029
[11]Department of Biochemistry and Molecular Biology, Indiana Univ School of Medicine, Indianapolis, IN 46202
[12]Child Health Institute, Robert Wood Johnson Medical School, Rutgers University, New Brunswick, NJ 08854

*Corresponding author:
Rutgers University
Department of Cell Biology & Neuroscience
604 Allison Rd
Piscataway, NJ 08854

(848) 445-1783
rhart@rutgers.edu

Abstract

Synonymous and noncoding single nucleotide polymorphisms (SNPs) in the *KCNJ6* gene, encoding G protein-gated inwardly rectifying potassium (GIRK2) channel subunit 2, have been linked with increased electroencephalographic frontal theta event-related oscillations (ERO) in subjects diagnosed with alcohol use disorder (AUD). To identify molecular and cellular mechanisms while retaining the appropriate genetic background, we generated induced excitatory glutamatergic neurons (iN) from iPSCs derived from four AUD-diagnosed subjects with *KCNJ6* variants ('Affected: AF') and four control subjects without variants ('Unaffected: UN'). Neurons were analyzed for changes in gene expression, morphology, excitability and physiological properties. Single cell RNA sequencing suggests that *KCNJ6* AF variant neurons have altered patterns of synaptic transmission and cell projection morphogenesis. Results confirm that AF neurons express lower levels of GIRK2, have greater neurite area, and elevated excitability. Interestingly, exposure to intoxicating concentrations of ethanol induces GIRK2 expression and reverses functional effects in AF neurons. Ectopic overexpression of GIRK2 alone mimics the effect of ethanol to normalize induced excitability. We conclude that *KCNJ6* variants decrease GIRK2 expression and increase excitability and that this effect can be minimized or reduced with ethanol.

63 # Introduction

64 Alcohol use disorder (AUD) is a heritable (h^2 = 0.49) condition characterized by an impaired
65 ability to stop or control alcohol use despite adverse social, occupational, or health
66 consequences[1]. An estimated 14.1 million American adults (ages 18+) were diagnosed with AUD
67 in 2019 and the numbers continue to grow, particularly due to the COVID-19 pandemic[2]. Even
68 though several evidence-based treatments are available for AUD[3-5], there is a high discrepancy
69 in treatment outcomes, suggesting the existence of a variety of traits influencing the
70 development of specific physiological and behavioral responses to alcohol. Understanding
71 biological factors, specifically genetic risk, at the level of neuronal function is fundamental to
72 developing tailored preventive interventions and better matching of patients to treatment.

73 The Collaborative Study on the Genetics of Alcoholism (COGA) collected a diverse set of
74 phenotypes, including electroencephalogram (EEG) parameters, in the search for genes and
75 endophenotypes associated with AUD[6, 7]. A family-based, genome-wide association study
76 (GWAS) of a frontal theta event related oscillation (ERO) phenotype identified an association
77 with several single nucleotide polymorphisms (SNPs), including a synonymous SNP, rs702859, in
78 the *KCNJ6* gene on chromosome 21[8]. More recent studies concluded that the rs702859
79 polymorphism influences the magnitude and topography of ERO theta power during reward
80 processing in a monetary gambling task, reflecting a genetic link to neuronal circuits[9, 10]. Two
81 other SNPs (rs702860 and rs2835872) within *KCNJ6* were linked with the ERO endophenotype
82 and AUD, but are noncoding, either intronic or within the 3' untranslated region (3' UTR),
83 respectively. Additional studies identified various genetic loci correlating with selected EEG
84 results but all consistently include alcohol dependence[11, 12]. To understand how these SNPs
85 might influence these phenotypes, it is essential to characterize the pathways and mechanisms
86 by which genetic risk unfolds at molecular, cellular and network resolutions. Furthermore, since
87 the *KCNJ6* SNPs are non-coding or synonymous, the optimal strategy would incorporate human
88 genetic backgrounds of actual subjects to preserve potential effects of noncoding sequences.

89 *KCNJ6* encodes the G protein-gated inwardly rectifying potassium channel subunit 2 (GIRK2),
90 which, when assembled into a GIRK channel, plays a role in regulating cell excitability[13]. The
91 inward rectifying properties of GIRK are based on the ability to conduct potassium ions into the
92 cell more easily than out, leading to a reduction in excitability[14, 15]. GIRK function in neurons is
93 associated with activation of G protein-coupled receptors (GPCRs), which leads to dissociation
94 of Gβγ subunits from the G protein complex and binding to the channel[16]. In addition, this
95 family of GIRK channels can be potentiated by ethanol concentrations (20-50 mM) relevant to
96 human alcohol usage through direct interaction with a hydrophobic pocket on the channel[17, 18].
97 Studies in model organisms also reveal the importance of GIRK function in AUD: mice lacking
98 GIRK2 demonstrate reduced ethanol analgesia, greater ethanol-stimulated activity in open-field
99 tests, increased self-administration of ethanol, and failure to develop a conditioned place
100 preference for ethanol[19-21]. Thus, GIRK channels not only modulate the excitability of the
101 neurons but also play an essential role in regulating responses to alcohol.

102 Recent studies have employed the use of subject-specific induced stem cell technology to
103 model, characterize and elucidate mechanisms underlying various types of addiction disorders
104 including AUD[22-25]. The generation of specific subtypes of cultured human neurons enables the
105 study of formerly inaccessible functional properties using standard neuroscience methods[22, 24-
106 26]. The contribution of various *KCNJ6* SNPs was found to affect a variety of properties
107 associated with neuronal function or sensitivity to drugs of abuse, suggesting targets for
108 potential therapeutic interventions. Associating specific genetic variants with mechanisms
109 contributing to addictive behaviors may produce more effective therapies tailored to individual
110 genotypes.

111 We hypothesize that noncoding SNP variants in *KCNJ6* alter neuronal excitability, potentially
112 contributing directly or indirectly to network-level endophenotypes such as ERO. Furthermore,
113 since ethanol interacts directly with GIRK2, we predict that excitability will be modulated by
114 ethanol. To test these hypotheses, we evaluated a human neuron model system that includes
115 variant genotypes, so that specific intergenic or noncoding sequences as well as modifying
116 genetic background influencing these functions would be preserved. Therefore, we selected
117 subjects from the NIAAA/COGA Sharing Repository, four with the ERO-associated allelic variant
118 in *KCNJ6* and the presence of diagnosed alcohol dependence and four without the variant and
119 unaffected for AUD and produced eight iPSC lines. iPSCs were reprogrammed into excitatory
120 human neurons (iN) to investigate the potential contribution of the *KCNJ6* SNPs to AUD
121 diagnosis and the ERO power endophenotype (Fig. 1A). We found that neurons from *KCNJ6*
122 variant AUD-affected individuals demonstrated initial transcriptomic and morpho-physiological
123 differences, mostly affecting excitability of the cells, which were paralleled by differences in
124 GIRK2 expression levels. Ethanol exposure, conversely, induced GIRK2 expression, ameliorating
125 differences in excitability. Moreover, by overexpressing *KCNJ6* we replicated effects of ethanol
126 on neuronal excitability. The results promote a better understanding of the association
127 between genetic variants and brain-wide changes affecting AUD risk and can potentially be
128 used for development of personalized interventions.

129

Methods

Generation of human iPS cells and glutamatergic neurons (iN)

Subjects were selected from the NIAAA/COGA Sharing Repository of the Collaborative Study on the Genetics of Alcoholism (COGA) project with characteristics summarized in Table 1. Selection criteria consisted of *KCNJ6* SNP genotype, DSM IV diagnosis of AUD, sex, and availability of frozen lymphocytes in the repository. All subjects were of European ancestry. Cryopreserved lymphocytes were reprogrammed to iPSC using Sendai-viral-expressed transcription factors (Oct3/4, Sox2, Klf4 and c-Myc; Cytotune™-iPS Reprogramming Kit, ThermoFisher) by RUCDR Infinite Biologics® (now Sampled, Inc.). Pluripotent cells were selected by colony morphology, alkaline phosphatase positivity, and immunocytochemical expression of Oct4 and TRA-1-60. Pluripotency was confirmed by colony morphology and immunocytochemistry for Oct4 and Tra-1-60 markers (Supplemental Fig. 1A). Identity of each iPSC line was confirmed by matching a 96 SNP panel to results obtained from fresh blood upon banking the original sample. Cultures were tested for mycoplasma (all negative) prior to release by RUCDR. Identities of the SNPs listed in Table 1 were confirmed in all iPSC lines by PCR amplification from genomic DNA and Sanger sequencing. Genomic integrity was confirmed using e-Karyotyping[27] using RNAseq data, which detected no anomalies (Supplemental Fig. 1B). Frozen aliquots were obtained for each subject, thawed, expanded, and maintained for neurogenesis. All iPS lines were cultured up to 50 passages for these experiments.

The previously-described protocol for generating glutamatergic human induced neurons (iN)[28-30] was modified. To obtain cultures with enhanced levels of spontaneous activity, we minimized the time of Ngn2 induction to reduce alternate cell identities[31] and fed cultures with a low-molality medium for at least 30 days post-induction[32]. Briefly, iPS cells were plated as dissociated cells on Matrigel® Matrix (Corning Life Sciences)-coated dishes in iPS-Brew-XF (StemMACS) medium supplemented with 2 µM Y-27632 (Peprotech, Inc.) and 2 ng/µl doxycycline, and infected with lentiviruses expressing Ngn2 (AddGene #52047) and rtTA (FUW-M2rtTA; AddGene # 20342) for 10–12h. The next day, the culture medium was replaced with Neurobasal medium/B27/GlutaMAX™ (Life Technologies) supplemented with 2 µg/mL of doxycycline (MP Biomedical), 2 µM Y-27632 and 2 ng/µl puromycin. Puromycin selection was continued for 2 days, and on day 5, the induced neurons were dissociated with Accutase (STEMCELL Technologies) and plated on Matrigel-covered glass coverslips with a monolayer of primary astrocytes (passage 2-3) isolated from postnatal day 0-1 mouse pups, as described previously[33]. Following plating, 50% of Neurobasal medium was changed to Neurobasal Plus culture medium with ascorbic acid, GlutaMAX, B27 Plus and Culture One supplements (Life Technologies). Half of the Neurobasal Plus medium with all supplements was replaced every 2–3 days. Cultures of iN typically exhibited resting membrane potentials averaging -40 mV with the presence of synaptic markers, spontaneous action potentials, and synaptic activity.

167 **Intermittent Ethanol Exposure (IEE).**
168 Since ethanol evaporates during culture incubation (Supplemental Figure 7), we initially added
169 ethanol to 20 mM and then replenished half the medium daily with 40 mM ethanol in medium.
170 Ethanol concentrations were measured using and AM1 Alcohol Analyzer (Analox Instruments,
171 Ltd.), as described previously[25].

172 **Primary mouse cortical neuron cultures**
173 P0-P1 mouse brains were obtained following decapitation on ice, meninges were removed,
174 cortex was dissected and cells were dissociated by incubation in trypsin (Gibco) for 5-7 min at
175 37°C. The cells were then washed with Hank's balanced salt solution (HBS) and triturated by
176 gentle pipetting. The cell suspension was centrifuged for 5 min at 160 x g and plated on
177 Matrigel-coated glass coverslips in Neurobasal medium/B27/L-Glutamine (Life Technologies).
178 When the density of glia in the culture reached ∼40–50% (approximately 2 days after plating),
179 50% of the conditioned culture medium was replaced with fresh medium containing 4 mM Ara-
180 C (Sigma; 2 mM final concentration). The cultures were maintained in medium containing 2 mM
181 Ara-C until fixation at 13–18 days in vitro (DIV).

182 **Generation of CRISPR/Cas9 Knockout iPSC**
183 As a negative control for GIRK2 antibody validation we generated a *KCNJ6* knockout by
184 CRISPR/Cas9 deletion in WTC-11, a publicly-available, control iPS line obtained from the
185 Gladstone Institute[34]. Two optimal gRNA targeting sequences were selected (using
186 http://crispr.mit.edu) to generate a frameshift 76-bp deletion, introducing three termination
187 codons within 40 bp following the deletion. A well-characterized iPSC line, WTB[35], was obtained
188 from the Gladstone Institute Stem Cell Core Facility (San Francisco, CA). Approximately 3 x 10^6
189 WTB iPSC (passage 58) were electroporated (amaxa Nucleofector) in suspension with a mixture
190 of two plasmids constructed from pSpCas9(BB)-T2A-GFP [AddGene #48138[36]], with sequences
191 targeting *KCNJ6*: G1, 5'-GATATCGGTCAGGTAGCGAT-3'; or G2, 5'-TCAGCCGAGATCGGACCAAA-3'.
192 One day after transfection, cells were dissociated with Accutase and sorted to select GFP^+ cells
193 into KSR medium (Life Technologies) with 2 µM Y-27632 and FGF (Peprotech, Inc.) and then
194 plated at low density into two wells of a 6-well plate. Approximately 7-10 days later, individual
195 colonies were hand-picked into 96-well plates. Three days after plating, cultures were split to
196 two 96-well plates. One plate was harvested at ~50-100% confluence for screening. Cells were
197 lysed in Quickextract (Lucigen), heated to 68°C for 6 minutes followed by 98°C for 2 minutes.
198 The lysate was PCR amplified (DET3-F: 5'- TGGACCCCAACACAGATTGG-3' and -R: 5'-
199 TGGATCAGGACGTCGAAAGC-3'), treated with exoSAPIT (Life Technologies) and analyzed by
200 agarose gel electrophoresis. From 96 colonies, approximately 19 appeared to have a single-
201 band deletion of the predicted size. Aliquots of the PCR reactions were sequenced with the F
202 primer to confirm. To confirm homozygosity, PCR products from four candidates were cloned
203 into a plasmid (StrataClone Blunt PCR Cloning Kit, Agilent) and individual colonies sequenced to
204 identify each allele. Only one candidate, A7, exhibited the designed homozygous 76 bp
205 deletion. A second colony with no deletion, E11, was selected to serve as unedited control.

206 **Bulk and single cell RNA sequencing**
207 For bulk RNAseq, individual iN cultures were harvested in lysis buffer and column purified
208 (Quick-RNA kit, Zymo). Purified RNA was sent to Novogene, Inc., for sequencing. Fastq files
209 were downloaded, filtered with Fastp[37], aligned to human reference genome (hg38) with
210 HISAT2[38], SNPs in mapped *KCNJ6* sequence were extracted using samtools mpileup[39] and
211 bcftools to filter for quality. Ensembl VEP[40] was used to annotate SNPs. RNAseq data have been
212 deposited with the NIH GEO repository (accession number GSE196491).

213 For single-cell RNA sequencing (scRNAseq), iN cultures were treated with 20 mM ethanol for 7
214 days using an intermittent ethanol exposure (IEE) protocol where alcohol was replenished daily
215 (Supplemental Fig. 7)[25]. At 28 days after plating onto glia, iN were dissociated using trypLE
216 Express (Thermo Fisher) for 5 minutes at 37°C. The dissociated cells were centrifuged at 200 x g
217 for 5 minutes at 4°C. The supernatant was removed, and cells were washed twice with 1X HBSS
218 (Thermo Fisher). After washes, cells were resuspended in 1% BSA (Bovine Serum Albumen,
219 ThermoFisher)/1xPBS (ThermoFisher). Cells were counted and resuspended at 1200 cells/µl in
220 1% BSA/ 1xPBS and placed on ice. Single-cell cDNA libraries were generated using the
221 Chromium Next GEM Single Cell 3 GEM Reagent Kits v3.1 (10X Genomics). Approximately
222 20,000 dissociated cells were loaded onto a cassette in the Chromium Controller with
223 accompanying reagents to generate Gel Beads in Emulsions (GEMs). GEMs were subjected to
224 reverse transcription to generate single-cell cDNA libraries before the oil emulsion was
225 disrupted and cDNA purified using Dynabeads MyOne Silane (Thermo Fisher). cDNA was
226 amplified by PCR for 11 cycles and purified using SPRIselect reagent (Beckman Coulter). cDNA
227 fragmentation, A-tailing, and end repair was performed followed by adapter ligation for paired-
228 end sequencing. An additional 11 cycles of PCR were performed to incorporate the sample
229 index sequences and to amplify the libraries before samples were purified using SPRIselect
230 reagent and used for sequencing. Libraries were shipped to Psomagen, Inc., for sequencing
231 service. Fastq files were downloaded, aligned with reference genome (initially hg38 and mm10)
232 using CellRanger (10XGenomics) and then imported into a Seurat (v. 4.0.6) object[41]. A summary
233 of human (GRCh38) and mouse (mm10) characteristics is shown in Supplemental Figure 2A and
234 CellRanger parameters are provided in Supplemental Table 2. Clusters of cells expressing
235 primarily mouse genes and therefore consistent with the co-cultured mouse glia was identified
236 (Supplemental Figure 2B) and removed. Human cells were isolated for further analysis. Cells
237 from individual subjects were identified using genome-wide SNPs that were expressed in the
238 mRNA. Demuxlet[42] assigned "best guess" identification by cell barcode, which was imported as
239 metadata into the human Seurat object. The number of identified cells was plotted for each
240 cell line and treatment (Supplemental Figures 2C). Seurat clusters consistent with neuronal
241 identity (Figure 1C, Supplemental Figure 2E) were selected for further analysis. Total numbers
242 of neurons by subject and treatment are plotted in Supplemental Figure 2D. A minimum of 10
243 cells per subject and treatment were required for analysis—only subject 351 in the control
244 condition fell below this threshold.

245 Differential gene expression was performed on gene counts aggregated by subject
246 ("pseudobulk" analysis). To exclude sporadically-expressed genes, detectable expression was
247 required in at least 25% of the cells in one group. After filtering, gene counts were summed for
248 each cell line and condition. Tables of summed gene counts were analyzed by DESeq2[43] using
249 the likelihood ratio test (LRT), comparing a model of groups to a reduced model. Contrasts
250 were calculated and significance required an adjusted p-value of 0.05 or less and at least a 1.5-
251 fold difference. Genes either up- or down-regulated were assessed for enriched gene ontology
252 biological process terms using the enrichGO function from the clusterProfiler package[44].

253 Summary data are listed in Supplemental Figure 2. These data have been deposited with the
254 NIH GEO archive, accession number GSE203530.

255 **Fluorescent in situ hybridization (FISH)**

256 Fluorescent, single molecule *in situ* hybridization was performed with the RNAscope® Multiplex
257 Fluorescent Detection Kit v2 (Advanced Cell Diagnostics, ACD) following the manufacturer's
258 instructions. In brief, iN cultures were fixed in 4% paraformaldehyde for 20 min at room
259 temperature, followed by a series of ethanol dehydration/rehydration steps, permeabilization
260 (with PBS-0.01% Tween buffer), blocking and overnight incubation with primary antibody
261 against MAP2 (Millipore AB5543, 1:100 dilution). Prior to probe hybridization, samples were
262 treated with hydrogen peroxide for 10 min and then with protease III (1:10) for 10 min. Human-
263 specific *KCNJ6* probe was hybridized for 2 h, followed by standard amplification and color
264 reaction with 520 Opal dye (Akoya Biosciences). MAP2 antibody was labeled with secondary
265 antibody (Alexa 633), nuclei were stained with DAPI, and coverslips were mounted on slides
266 using mounting medium (Thermo Fisher). Images were acquired on a Zeiss LSM 800 confocal
267 microscope using a 40x objective. *KCNJ6* was quantified by manually counting fluorescent
268 puncta within the MAP2/DAPI positive regions of individual neurons (defined as "somatic") or
269 as puncta scattered along the MAP2-associated processes ("non-somatic"). Levels of *KCNJ6*
270 were binned according to semi-quantitative histological scoring methodology by levels using
271 Advanced Cell Diagnostics scoring criteria, where low expression of RNA target was defined to
272 be 1-3 puncta per cell, intermediate 4-9, high 10-15 and very high >15 per cell.

273 **Electrophysiology**

274 Functional analyses of induced human neurons were performed using whole-cell patch-clamp
275 electrophysiology as previously described[24, 25]. Recordings were done in HEPES buffer consisting
276 of (in mM): 140 NaCl, 5 KCl, 2 $CaCl_2$, 2 $MgCl_2$, 10 HEPES, 10 Glucose. Osmolality of the buffer
277 was between 290-305 mOsm and the pH was adjusted to 7.4. Whole-cell patch-clamp
278 recordings were performed using borosilicate glass electrodes with resistances of 4-8 MΩ and
279 intracellular solution containing the following (in mM): 126 K-Gluconate, 4 KCl, 10 HEPES, 4
280 ATP-Mg, 0.3 GTP-Na_2, 10 Phosphocreatine, with pH adjusted to 7.2 and osmolarity to 270−290
281 mOsm. After patching, neurons were allowed to rest for 5-7 min, or until the RMP drift
282 stabilized, before recording. For GIRK2 channel recordings, an extracellular solution with high K^+
283 was used, which consisted of: 20 mM KCl, 140 mM NaCl, 2 mM $CaCl_2$, 2 mM $MgCl_2$ and 10 mM

284 HEPES (pH 7.4). GIRK-mediated currents were measured at -40 mV membrane potential
285 holding. Excitability of the neurons was measured by applying ramp (+200 pA) and step (-50 pA
286 – 100 pA) depolarizing pulses while holding neurons at -65mV (current clamp mode). All
287 recordings in cultured human neurons were performed at room temperature. Cells were
288 excluded from analysis if access resistance changed by more than 20% across the duration of
289 the recording. For current injection studies, neurons were excluded if RMP was close to -63mV
290 and the required current injection was less than 1 pA (absolute value). In addition, any induced
291 neurons whose access resistance was greater than 35 MΩ were also excluded. Drugs were
292 applied through a perfusion system in the following concentrations: 160 nM ML297 or 20 mM
293 alcohol. Clampfit software (pClamp 11; Molecular Devices) was used for analysis of recordings.

294 **Immunocytochemistry and confocal imaging**

295 iN cultures were fixed for 30 min in ice cold methanol and permeabilized using 0.2% Triton X-
296 100 in PBS for 15 min at room temperature. Cells were then incubated in blocking buffer (5%
297 BSA with 5% normal goat serum in PBS) for 30 min at room temperature and then incubated
298 with primary antibodies diluted in blocking buffer overnight at 4°C, washed with PBS three
299 times, and subsequently incubated with secondary antibodies for 1 h at room temperature.
300 Confocal imaging analysis was performed using a Zeiss LSM700. Primary antibodies used: rabbit
301 anti-GIRK2 (Alomone labs, APC-006, 1:400), mouse anti-βIII-tub (Bio legend, MMS-
302 435P,1:1000), chicken anti-MAP2 (Millipore AB5543, 1:1000), mouse anti-Syn1 (SYSY,106-011,
303 1:200), mouse anti-PSD 95 (SYSY, 124-011, 1:2000), mouse anti-mCherry (Thermofisher
304 Scientific, M11217, 1:100).

305 **Validation of GIRK2 immunoreactivity**

306 To validate the specificity of GIRK2 detection, GIRK2 was overexpressed by transduction with a
307 ubiquitin C (UbiC) promoter-driven, *KCNJ6*-expressing lentivirus or expression was eliminated
308 by introducing frameshift deletions into *KCNJ6* using CRISPR/Cas9-editing. Overexpression was
309 initiated by infection on day 27 post-induction and GIRK2 expression was evaluated 14 days
310 later. Levels of GIRK2 in iN prepared from the CRISPR/Cas9 knockout line were measured at a
311 similar time post-induction (~day 40). Viral GIRK2 transduction was confirmed by co-expression
312 of mCherry.

313 **Image analysis**

314 Cytometric analysis of confocal images of MAP2-stained iN cultures was performed using the
315 Fiji/ImageJ image analysis program[45]. Regions of Interest (ROIs) were created for each cell by
316 encapsulating the cell body through use of the cell magic wand tool. The cell body was then
317 quantified for area and shape descriptors. The NeurphologyJ Fiji macro[46] was utilized for
318 detection and quantification of extended neuronal morphometry. A threshold was selected
319 manually so that most neurites are well-defined without significant particle detection or noise.
320 GIRK2 puncta quantification used trainable Weka Segmentation[47] to segment the image to
321 establish two classes. One class identified pixels that corresponded to GIRK2 puncta for
322 intensity, circularity, and size. A second class identified pixels that did not correspond to puncta,

323 such as noise from neurons and background. The classifier was trained multiple times until
324 there was a high confidence that the pixels segmented into class one had a high (90%)
325 confidence interval denoted by probability maps. The segmented image was adjusted to
326 remove any false negatives. The class one binary image was then used for puncta cytometry.
327 ImageJ scripts can be downloaded from https://github.com/rhart604/imagej. The person
328 performing analysis was given coded images with no genotype or line information so that
329 analysis would be blinded.

330 **Lentiviruses**

331 FSW-hSyn-GCaMP6f assembly was described previously[48]. FUGW-KCNJ6-mCherry was
332 assembled using lentiviral backbone from FUGW (AddGene #14883), *KCNJ6* coding sequence
333 amplified from human neuron cDNA (forward primer: agccaggaaaagcacaaaga, reverse primer:
334 ggggagaagagaagggtttg), and mCherry with a nuclear localization signal from pME-nlsmCherry (a
335 gift from Dr. Kelvin Kwan). During construction, the GIRK2 protein-coding sequence was tagged
336 with a 3xHA tag and linked to mCherry with a T2A "self-cleaving" element.

337 **Calcium imaging in iPSC-derived iN populations**

338 For assessing neuronal excitability, iN co-cultured with mouse glia on Matrigel™ coated 10 mm
339 glass coverslips were transduced with lentivirus expressing hSyn-GCaMP6f at least 2 weeks
340 prior to imaging to ensure robust expression. All fluorescence imaging experiments were
341 performed in ~50 DIV (days in vitro) iNs. Coverslips were mounted on a diamond-shaped
342 chamber and placed on a Nikon Eclipse TE2000-U microscope with a 10X objective. GCaMP6f
343 was excited using a 480 nm (Mic-LED-480A, Prizmatix), a HQ480/40x excitation filter, a Q505LP
344 dichroic mirror, and a HQ535/50m emission filter (Semrock). Fluorescence was projected onto a
345 sCMOS Zyla 5.5 camera (Andor) and sampled at a rate of 4.7 fps with a frame exposure of 200
346 ms at 160x120 pixels (4x4 binning). Light source and sCMOS camera were controlled with the
347 Nikon Elements software (NIS-Elements AR 5.20.01).

348 Neurons were continuously perfused during fluorescence recording with ACSF with the
349 following composition (in mM): NaCl 125, KCl 5, D-Glucose 10, HEPES-Na 10, $CaCl_2$ 3.1 and
350 $MgCl_2$ 1.3. The pH was adjusted to 7.4 with HCl and osmolarity corrected with sucrose to 290-
351 300 mOsm. Depolarizing solutions were prepared in ACSF with 10 or 50 µM glutamate, or with
352 18 mM KCl. Perfusion was gravity fed (flow rate of 0.065 ml/s). Solution exchanges were
353 controlled with a ValveBank8 II (AutoMate Scientific Inc.). Calcium transients were recorded
354 using a protocol based on glutamate and KCl perfusion, that consisted of 3 min baseline activity
355 (ACSF), 3 x 30 s pulses of 10 µM glutamate (30 s ACSF between pulses), one 30 s pulse of 50 µM
356 glutamate, 2 min of ACSF wash, 3 x 30 s pulses of 18 mM KCl (30 s ACSF between pulses), and a
357 final ACSF wash for 5 min (Fig. 4C).

358 ROI segmentation of GCaMP6f-expressing neurons, raw fluorescence extraction and
359 background correction were performed with Nikon Elements software. ΔF/F was calculated
360 with the formula $(F_t - F_{min})/F_{min}$, where F_t is the raw fluorescence at time t and F_{min} is the
361 minimum fluorescence for the entire trace. The resulting trace was then denoised with a low-

362 pass Butterworth filter and baseline corrected for drift using an adaptative iteratively
363 reweighted Penalized Least Squares (AirPLS) based algorithm [49], in R-studio (R version 4.0.3).
364 Peak detection was performed using a custom script in R that considered neuron action
365 potential-derived Ca^{2+} spikes that had the following criteria (for a framerate acquisition of 4.7
366 fps): duration < 30 frames, rise phase >= 2 frames, fall phase >= 5 frames, rise phase < fall
367 phase, peak height > 5*SD, and peak height > 5*max background signal. The analysis pipeline is
368 depicted in Supp. Fig. 6. Statistical analysis was performed in GraphPad Prism 8.4.3 or R version
369 4.0.3.

370 **Statistics**

371 Parameters that were sampled in cells from multiple microscopic fields and from multiple cell
372 lines were fit to a linear mixed-effects model using the lme4 package in R[50]. The model included
373 the cell line identifier and sex. A Tukey post-hoc test identified pairwise differences in two-
374 factor models (e.g., combined genotype and ethanol exposure). Electrophysiology results were
375 modeled using generalized estimating equations (GEE) with the cell line as grouping identifier
376 using the geepack R package[51]. Where appropriate, ANOVA or Student's t-test was used as
377 indicated in figure legends. For RNAseq, pseudo-bulk data (single cell reads pooled by subject
378 identifier) were modeled in DESeq2[43], testing first by likelihood ratio testing (LRT) over all
379 groups, and then pairwise comparisons were evaluated using Wald tests. After Benjamini-
380 Hochberg multiple measurements correction, a false discovery rate of 5% was set as a
381 threshold for significance. Numbers of replicate cells and/or fields per cell line and genotype
382 used for statistical testing are listed in Supplemental Table 6.

383

Results

Gene expression patterns predict functional differences between iN generated from AUD affected and unaffected individuals

To investigate the role of *KCNJ6* gene variants in neuronal function and ethanol response we selected a balanced set of eight subjects of European ancestry from the COGA cell repository, with contrasting *KCNJ6* SNPs and the presence or absence of alcohol dependence (Table 1). Since multiple SNP genotypes were used, we label groups as AUD "affected" (**AF**) or "unaffected" (**UF**) for simplicity, since in this set of subjects diagnosis correlates with the SNP haplotype. However, the focus of this study is the *KCNJ6* haplotype.

To confirm and extend SNP genotypes in the two groups, iN cultures from each cell line were harvested for bulk RNAseq analysis. To identify RNA isoforms, genome-aligned RNAseq data identified only the longer *KCNJ6* transcript isoform ENST00000609713 (Fig. 1B), which includes a 3' exon of 18,112 nucleotides that primarily consists of noncoding 3'UTR. Genotypes for the two exonic SNPs (Table 1) were confirmed for all eight cell lines, but we also identified an additional 19 noncoding, 3'UTR SNPs linked with the initial three (Supplementary Table 1; mapped with red lines in Fig. 1B), constituting a haplotype of 22 variants (synonymous and noncoding) within the expressed isoform of *KCNJ6* mRNA, all in a region of linkage disequilibrium (LD; Supplemental Figure 1C). There are no nonsynonymous variants in either haplotype, therefore, any function would be predicted to affect *KCNJ6* mRNA stability, translation, or other post-transcriptional processes.

Group	ID	Sex	DSMIV Dx	rs702859 Synonymous	rs702860 Intronic	rs2835872 Intronic
AF	376	M	Affected	GG	GG	AA
	246	M	Affected	GG	GG	AA
	351	F	Affected	GG	GG	AA
	233	F	Affected	GG	GG	AA
UN	472	M	Unaffected	AA	AA	GG
	384	M	Unaffected	AA	AA	GG
	451	F	Unaffected	AA	AA	GG
	420	F	Unaffected	AA	AA	GG

Table 1. Subjects selected for iPSC. The ID is a three-digit code that is not traceable to the subject identity. Genotypes for listed SNPs were obtained from GWAS studies[8]. SNP genotypes were confirmed by iPSC genomic DNA PCR and Sanger sequencing.

To enable selective analysis of the more appropriately induced neurons, we used single-cell RNAseq (scRNAseq) of pooled neurons from multiple cell lines, a strategy known as a "cell village[52]." Based on preliminary results indicating differences in synaptic activity, we cultured each group separately, to avoid potential secondary effects due to differential synaptic activity, combining cells from all 4 lines within each group in equivalent proportions. Previous functional studies suggested that iN cultures may be heterogeneous, potentially confounding a bulk

413 RNAseq analysis[31]. Following maturation (~30 days after induction), dissociated cells were
414 processed to generate scRNAseq libraries. Mapping cells by t-distributed stochastic neighbor
415 embedding (tSNE), a distinct cluster of cells coordinately expressed several markers consistent
416 with neuron physiological function (Fig. 1C and Supplemental Fig. 2E), including synaptic marker
417 (*SYP*), voltage-gated sodium channel (*SCN3A*), glutamate transporter (*SLC17A6*), and both
418 NMDA (*GRIN2A*, *GRIN2B, GRIA2, GRIA4*) and kainate glutamate receptors (*GRIK2*). This cluster
419 also expressed both *KCNJ6*, encoding GIRK2, and *KCNJ3*, encoding GIRK1, which are required to
420 form heterotetrameric, functional channels[14, 53]. Detection of mRNA expression in individual
421 cells by scRNAseq is likely an underestimate due to the relatively small number of reads per
422 cells, so the cluster identified as neurons is likely to express markers more uniformly than
423 observed here. We conclude that this subset of cells represents those expressing components
424 required for neuron physiological activity, and that other, sporadic cells, expressing subsets of
425 these neuronal markers, are likely alternate products of induction, which we label as
426 "transitional" neurons (Fig. 1C), since reprogramming is not identical to differentiation[54, 55].
427 Therefore, we focused gene expression analysis on the phenotypically neuronal subset of cells.

428 Cells from individual subjects were distinguished by expressed SNP profiles[42], and sequencing
429 reads of cells from each subject were combined to create a "pseudo-bulk" analysis, treating
430 each subject and treatment condition as a single replicate. Comparing the untreated AF group
431 with the untreated UN group, we identified 797 genes up-regulated, and 596 genes down-
432 regulated (Fig. 1D; Supplemental Table 3). Examining the results for differences by sex instead
433 of *KCNJ6* haplotype identified only 6 genes, of which 4 are encoded on X or Y chromosomes,
434 indicating that the sex of the samples did not substantially contribute to gene expression
435 differences. Gene ontology analysis of the down-regulated genes (Fig. 1E; Supplemental Table
436 4-5) predicts several biological processes associated with nervous system development, axonal
437 transport, trans-synaptic signaling and others. By grouping enriched gene ontology terms into a
438 tree plot by their parent terms (Supplemental Fig. 3), the major themes in the down-regulated
439 genes (AF < UN; Supplemental Table 5) are synaptic signaling and neuro projection
440 morphogenesis. Up-regulated genes (AF > UN; Fig. 1E; Supplemental Table 4) predict functions
441 associated with protein targeting within the cells, catabolic metabolism, and nonsense-
442 mediated decay. The level of *KCNJ6* mRNA trended lower in untreated AF than in UN (Fig. 1C; p
443 $= 3.15 \times 10^{-5}$ by LRT over both genotype and ethanol treatment; $p = 0.0508$ for untreated AF vs.
444 UN by Wald test). Interestingly, 7 d of 20 mM IEE increased levels of *KCNJ6* mRNA (Fig. 1C; $p =$
445 0.0225, Wald test) so that the treated AF group was no longer different from untreated UN ($p =$
446 0.322; Wald test). Analysis by sex identified no significant difference in *KCNJ6* mRNA. Results
447 indicate that the variant *KCNJ6* haplotype leads to differential expression of GIRK2 and that
448 ethanol exposure will reverse these effects.

449 **GIRK2 expression and function in iPSC-derived induced excitatory human neurons (iN)**
450 Given the differences in gene expression and partial reversal of KCNJ6 downregulation, we
451 evaluated detailed neuronal phenotypes in UN and AF iN cultures, including GIRK2 expression,
452 neuronal morphology, and physiological response. Since GIRK2 immunocytochemistry had not

453 been reported in cultured human neurons, we validated detection using mouse primary cortical
454 cultures[56]. GIRK2 immunoreactivity in human iNs matched a pattern of process-selective
455 expression in mouse (Fig. 2A, Supplemental Fig. 4A), where GIRK2 was detected as relatively
456 small (~ 0.5 µm diameter) puncta scattered primarily along the processes (Fig. 2B). Importantly,
457 silencing KCNJ6 with shRNAs or frameshift knockout by CRISPR/Cas9 eliminated GIRK2
458 immunoreactivity (Supplemental Fig. 4B,C). Localization of GIRK2 immunoreactivity in human iN
459 did not directly colocalize with synaptic vesicle marker VGLUT2 or synaptic marker Syn1
460 (Supplemental Fig. 5), but instead was found most frequently adjacent to synapses but
461 overlapping the shafts of the βIII tubulin-positive processes, and less so on MAP2 positive
462 processes (Figs. 2D.a, 3C, 3E). Cultured neurons express βIII tubulin throughout the cell, but not
463 as strongly in axonal processes[57]. We previously found that processes in human iN cells stained
464 for ankyrin G, identifying the axonal initial segment, which similarly lacked βIII-tubulin[58].
465 Detection of GIRK2 primarily on βIII-tubulin$^+$/MAP$^-$ processes, therefore, suggests pre-axonal,
466 and likely presynaptic, localization. Results confirm that lentiviral-transduced GIRK2
467 overexpression increased levels of immunostaining about 3.5-fold (Fig. 2C, mCherry$^+$ cells are
468 KCNJ6 lentiviral-transduced) which further confirms antibody specificity.

469 To confirm that GIRK2 expression contributes to potassium channel function, we treated iN
470 cultures with ML297, a selective activator of the GIRK1/GIRK2 heterotetramer complex[59, 60].
471 Results show that the magnitude and frequency of native (basal) currents observed in human iN
472 were relatively small (Fig. 2D.b), with only 6.8% of the neurons responding to a shift in
473 membrane potential holding current (~10 pA). This agrees well with immunocytochemical data
474 showing that GIRK2 expression is relatively low and with scRNAseq detection of *KCNJ6* in a
475 subset of cells (Fig. 1C). However, by recording from cells overexpressing GIRK2 (identified by
476 mCherry co-expression; Fig. 2D.c), we found an increased frequency of response (GIRK currents)
477 to 30% of the cells after ML297 addition (Fig. 2D.b) without a change in magnitude (Fig. 2D.e).
478 Importantly, we also found that GIRK activation affected excitability of the neurons by shifting
479 resting membrane potential to more negative values (Fig. 2D.d), thus affecting the ability of
480 neurons to fire APs when induced (Fig. 2D.f). We conclude that increased *KCNJ6* expression
481 affects neuronal excitability by altering GIRK channel activity.

482 ***KCNJ6* haplotype alters morphology and membrane excitability in human iNs**

483 To identify neuronal properties affected by *KCNJ6* haplotype, we focused on three aspects:
484 morphology, expression of GIRK2, and basal physiological properties. A detailed analysis of
485 neuronal morphology is essential to rule out differences affecting excitability[61]. Most measures
486 of basic neuronal morphology did not exhibit statistically significant differences by group,
487 including soma size, circularity, and solidity, which describe the most fundamental aspects of
488 neuron shape (Fig. 3B.a-c). However, neurite area, as determined by βIII-tubulin-stained area,
489 reflecting the number and/or branching of neurites per cell, increased in the AF group (p
490 =0.018; Fig. 3B.d), with example images shown for individual cell lines in Figure 3C. Results are
491 plotted for each cell line or aggregated by *KCNJ6* haplotype from multiple cell lines. As

492 predicted by the scRNAseq expression of *KCNJ6* mRNA (Fig. 1J), GIRK2 immunoreactivity was
493 decreased in the AF group (Fig. 3D), as measured by puncta counts ($p = 0.0012$; Fig. 3D.a),
494 puncta circularity ($p = 0.007$; Fig. 3D.c), and solidity ($p = 0.037$; Fig. 3D.d) but not puncta size
495 (Fig. 3D.b). No difference was found by sex. Sample GIRK2 puncta are shown for each cell line in
496 Figure 3E. These results demonstrate an overall decrease in GIRK2 in neuronal processes in the
497 AF (*KCNJ6* variant allele) group.

498 Reduced GIRK2 expression is predicted to affect the excitability of neurons. As expected, we
499 found no differences in membrane capacitance, membrane resistance, spontaneous excitatory
500 post-synaptic potential (sEPSC) frequencies or amplitudes, or spontaneous action potential (AP)
501 firing (Fig. 3F). However, we observed a significant increase in excitability in the AF group ($p =$
502 1.2×10^{-5}, Fig. 3G). Less current injection, using a ramp technique, was required for the AF
503 group to shift the resting membrane potential (RMP) of neurons held at -65 mV, producing
504 more AP firing, compared with the UN group ($p = 2.0 \times 10^{-9}$, Fig. 3G.d). Therefore, the *KCNJ6*
505 variant haplotype group (AF) exhibited increased neurite area, reduced neurite GIRK2
506 expression, and greater excitability. Other neuronal properties were not different across the
507 two groups, suggesting that overall neuron differentiation status was similar.

508 Electrophysiology was assessed in multiple individual cells, but since cultures are
509 heterogeneous (Fig. 1C), we wished to evaluate larger samples of cultures. Therefore, to
510 confirm that the observed effects are consistent across larger populations of cells, we used
511 calcium imaging to assess spontaneous and glutamate-stimulated firing. We selected four cell
512 lines for these studies (AF: 233 and 246, and UN: 420 and 472) and used the viral-transduced,
513 genetically-encoded calcium indicator GCaMP6f as a proxy for neuronal activity[62]. Example
514 images show consistent expression in all cell lines (Fig. 4A). Cultures were treated with
515 repeated pulses of 10 μM glutamate (each followed by wash-out with ACSF), and one pulse of
516 50 μM glutamate to elicit transient increases in fluorescence, indicating receptor-induced
517 excitability, followed by pulses of 18 mM KCl, indicating cellular excitability (Fig. 4B-D). Neurons
518 from both UN and AF groups had heterogeneous spiking patterns, with >50% of the neurons
519 remaining inactive during the baseline period or after stimulation with glutamate or KCl. This is
520 consistent with scRNAseq results indicating that only ~23% of the iN cells express genetic
521 markers consistent with excitability (Fig. 1C). Increased spontaneous and induced spiking (> 1-2
522 spikes) was apparent in the AF group when viewing individual cell responses in a raster plot
523 (Fig. 4B-C). Spiking frequencies increased 2.4-fold in baseline conditions (Fig. 4E; $p = 1.1 \times 10^{-6}$)
524 and 1.3-fold following glutamate stimulation (Fig. 4F; $p = 1.6 \times 10^{-3}$) in the AF group, but no
525 difference was found in KCl-induced activity (Fig. 4G; $p = 0.85$), confirming the above results
526 from individual neurons. When examining the AF or UN neurons individually, we also observed
527 higher spontaneous and glutamate elicited excitability for lines 233 and 246 when compared to
528 line 472, which was found to be the least active spontaneously or under glutamate stimulation
529 among the four studied with this imaging approach (Supp. Fig. 6). Overall, cells from the AF
530 *KCNJ6* variant allele group were more excitable, with no difference in basal physiological

531 properties (i.e., KCl-induced activity). Furthermore, not only did the spike rate increase per cell
532 (bar plots, Spikes/ROI/min), but we also observed increases in the proportion of cells in a field
533 that responded (pie plots). These results not only confirm earlier findings of differences in
534 excitability, but also demonstrate that the difference in the AF iNs is found in not only individual
535 cell activity but also in the frequency of detecting active cells within a population.

536 **Ethanol exposure eliminates differences in neuronal properties affected by *KCNJ6* haplotype**
537 Analysis of *KCNJ6* mRNA expression in selected neurons (Fig. 1C) not only detected decreased
538 basal levels in the AF group, but also demonstrated increased expression following ethanol
539 treatment (~2-fold increased, p = 0.0225 Wald test). This result predicts that increasing GIRK2
540 expression in the AF group following ethanol treatment would eliminate differences from the
541 UN group in morphology, expression, and physiology.

542 To control ethanol dosage in culture, we utilized an intermittent ethanol exposure (IEE)
543 paradigm as in previous studies[25]. We replenished ethanol daily to account for loss by
544 evaporation, producing measured concentrations with a mean of 15.4 ± 1.16 mM
545 (Supplemental Fig. 7). We determined that the half-life of ethanol is 14.5 h (with a 95% CI of
546 13.5 to 15.6 h), so over 24 h the concentration would drop to ~5-8 mM before replenishment.
547 We targeted a peak concentration of 20 mM ethanol, which is similar to a blood alcohol
548 concentration (BAC) of 0.08% (17 mM), the legal limit for intoxication. We also selected this
549 concentration based on the reported concentration-dependent interaction of GIRK2 with
550 ethanol[17]. After 7 days of IEE, we evaluated neuronal morphological and functional properties.
551 Focusing on those parameters that were different by genotype without IEE (Fig. 3&4), we found
552 that ethanol eliminated the differences in total neurite area (not significant; p = 0.98, Fig. 5A.d),
553 GIRK2 puncta counts (p = 0.46, Fig. 5B.a), excitation following current injection (p = 0.32, Fig.
554 5E.a), step- (p = 0.48, Fig. 5E.b), and ramp- (p = 0.95, Fig. 5E.d) induced APs. Membrane
555 capacitance was slightly but significantly reduced in the IEE AF group ($p = 9.6 \times 10^{-9}$, Fig. 5D.a).
556 Other measurements were unchanged, again indicating that the cultured neurons exhibited
557 similar differentiation properties. Results are consistent with the interpretation that neurite
558 and excitability differences correlate with reduced GIRK2 expression, and that ethanol increases
559 expression of GIRK2, potentially reversing these effects.

560 To confirm that both *KCNJ6* haplotype and ethanol exposure affect GIRK2 expression, we
561 evaluated GIRK2 immunocytochemistry and *KCNJ6* mRNA in neurons using fluorescent in situ
562 hybridization (FISH). GIRK2 increased following IEE ($p=1.0 \times 10^{-20}$, Fig. 5G-H). By probing *KCNJ6*
563 fluorescent puncta colocalized with MAP2 immunocytochemistry, we confirmed that neurons
564 from AF individuals had lower levels of *KCNJ6* mRNA expression compared to UN neurons (Fig.
565 5J.a, $p = 8.2 \times 10^{-3}$). We also found that the proportion of $MAP2^{+}$ neurons expressing KCNJ6 was
566 reduced in AF compared with UN (50.1% vs 64.7%, Fig. 5J.b), and the AF neurons had a greater
567 proportion of cells with low levels of expression (Fig. 5J.c) with no detectable High or Very High
568 (>9 puncta/cell) expression. Differences in expression were found by haplotype in somatic
569 regions of neurons (Fig. 5J.f, $p = 5.5 \times 10^{-3}$) but not in non-somatic processes (Fig. 5J.g, p = 0.23).

570 Ethanol increased *KCNJ6* mRNA levels in both groups (Fig. 5J.a-e), eliminating the difference
571 between genotypes. Interestingly, we also observed that the proportions of AF neurons
572 expressing KCNJ6 was increased (8.3%, Fig. 5J.b) by ethanol and was paralleled by a reduction in
573 number of low-expressing cells and increased appearance of high-expressing neurons (Fig. 5J.c).
574 Results indicate that variant *KCNJ6* haplotype leads to reduced *KCNJ6* expression, which is
575 consistent with RNA sequencing and immunocytochemical results, and that ethanol increases
576 *KCNJ6* expression, eliminating differences between haplotype groups.

577 **GIRK2 overexpression mimics IEE in human neurons with *KCNJ6* variants**

578 To test if ethanol-induced GIRK2 expression could underlie the elimination of differences in
579 neuronal properties associated with the *KCNJ6* haplotype, we compared ethanol treatment
580 with virus transduced *KCNJ6* overexpression. Since ethanol has been shown to potentiate
581 GIRK2-containing channels, we used a single treatment with 20 mM ethanol followed by
582 fixation 24 h later. As expected, neither ethanol nor GIRK2 overexpression exhibited differences
583 in passive neuronal properties. However, while current-induced activity increased in control
584 cultures ($p = 6.8 \times 10^{-6}$, Fig. 6C), no significant difference was found in cultures exposed to 24 h
585 ethanol ($p = 0.74$) and GIRK2 overexpression ($p = 0.23$). Similarly, while control cultures had
586 increased ramp-induced APs ($p = 5.9 \times 10^{-4}$; Fig. 6A) neither GIRK overexpression ($p = 0.14$) or
587 ethanol ($p = 0.10$) were significantly different. As a control, GIRK2 puncta count increased in a
588 sample cell line after overexpression (line 376, $p = 0.04$, Fig. 6D) without an increase in
589 circularity or solidity (not shown). These results indicate that the increased excitability in *KCNJ6*
590 minor allele haplotype cells is due to reduced expression of GIRK2 protein and this effect is at
591 least partially ameliorated or reversed by exposure to doses of ethanol found in human brain
592 after moderate to heavy daily drinking.

593

Discussion

This study focused on the effect of an AUD- and endophenotype-linked *KCNJ6* haplotype on neuronal function, with a goal of identifying mechanisms that could eventually drive therapeutic strategies. To retain the appropriate genetic background for individuals with AUD, we selected subjects from the large NIAAA/COGA Sharing Repository, using both the selected *KCNJ6* haplotype and diagnosed alcohol dependence as criteria (Table 1). By preparing iPSC from these subjects and inducing them to model excitatory neurons, we identified differences in *KCNJ6* mRNA levels and GIRK2 immunoreactivity in individuals with variant *KCNJ6* haplotypes. Gene expression differences predicted effects on neuronal signaling including synaptic function. The *KCNJ6* haplotype was also associated with differences in the area of βIII-tubulin^{+} neuron projections and membrane excitability, but not in other measures of neuronal differentiation. Surprisingly, we found that ethanol exposure led to an increase in *KCNJ6* mRNA and GIRK2 expression, paralleled by a reduction or elimination of morphological and physiological differences in these neurons. Reversal of *KCNJ6* haplotype effects by ethanol could also be mimicked by overexpressing GIRK2. These results demonstrate that genetic variants enhancing risk of AUD, even if they do not alter protein sequence, can trigger neuronal mechanisms at the cellular level mirroring or predicting endophenotypes, here ERO, linked with AUD behavior.

Non-coding *KCNJ6* polymorphisms in AUD

Most GWAS SNPs map to non-coding regions of the genome and 3.7% are found in the UTRs[63, 64]. The 3′ UTRs of transcripts that are expressed in the brain tend to be longer than those expressed in other tissues and can be involved in post-transcriptional regulation of transcript abundance by affecting RNA stability, translation and/or localization[65, 66]. Reference genome annotation of *KCNJ6* identifies two transcripts, one with a short 3' UTR (1,926 bp; Ensembl ENST00000645093, RefSeq NM_002240) and one with a substantially longer 3' UTR (18,112 bp; Ensembl ENST00000609713). RNAseq coverage analysis in human iN cultures detects only the longer isoform, although it is possible that a relatively small portion could be the shorter isoform, but the uniformly distributed coverage (Fig. 1B) does not indicate this. This longer transcript is orthologous to a 16-kb transcript found in rat brain[67], which includes multiple AU-rich elements, which may affect mRNA stability and could be affected by *KCNJ6* allelic variation. We conclude that the vast majority of *KCNJ6* mRNA is consistent with having the extended 3' UTR, with the potential for variant SNPs to affect mRNA stability or translation efficiency.

In addition to the three synonymous and intronic SNPs used to select subjects (Table 1), examination of variants in the long 3'UTR by RNAseq alignment predicts linkage of 19 additional SNPs (Fig. 1B; Supplemental Table 1). None of the 3' UTR SNPs could be mapped uniquely to known regulatory sequences such as predicted microRNA target sites. That is, some SNPs are predicted to destroy or add predicted targeting sites, but all of these potential target sites were found in multiple locations within the 3' UTR, not only where they might be altered by a SNP. It is possible, however, that altered microRNA targeting of one or more sites among many in the

633 3'UTR could play a role in regulating the stability or translation of the variant *KCNJ6* mRNA, but
634 no clear candidates could be identified for testing. Furthermore, since ethanol exposure of
635 neurons has been found to inhibit 1-carbon metabolic pathways, leading to selective changes in
636 histone methylation[68], it remains possible that a sequence-specific epigenetic mechanism other
637 than microRNAs may affect *KCNJ6* variant expression.

638 However, results demonstrate that the non-coding variant haplotype alters expression of GIRK2
639 protein and *KCNJ6* mRNA. We found that iN from subjects with the homozygous variant *KCNJ6*
640 haplotype exhibited lower expression of GIRK2 by immunocytochemistry (Fig. 3D), but while
641 the difference in neuronal mRNA levels as detected by scRNAseq analysis matched this trend, it
642 did not reach significance ($p = 0.0508$; Fig. 1C). FISH analysis, however, confirmed that *KCNJ6*
643 mRNA was reduced in the AF group (Fig. 5J). *KCNJ6* mRNA was also detected in fewer $MAP2^+$
644 cells and at lower levels per cell (Fig. 5J.b-c). The results of counting GIRK2 puncta and
645 evaluating *KCNJ6* mRNA by scRNAseq and FISH support a diminished expression of GIRK2 in
646 neurons from the affected group.

647 The secondary effects of *KCNJ6* mRNA and GIRK2 protein regulation include many predictors of
648 altered neuronal connectivity and signaling. Genes that were reduced in the AF group (GO:BP
649 Down in Fig. 1E; Supplemental Fig. 3B) point to changes in synaptic transmission and projection
650 morphology. The tree plots in Supp. Fig. 3B are particularly useful to group GO terms by their
651 parent terms and to judge the numbers of genes affected (by the diameters of the circles
652 plotted). Since we focused on *KCNJ6* haplotype differences in cells without ethanol, we did not
653 expect to match findings in, for example, human AUD brains[69], which found prominent effects
654 in astrocytes and microglia.

655 Surprisingly, ethanol exposure increased expression of both GIRK2 immunoreactivity and *KCNJ6*
656 mRNA. Following 7 days of IEE with a peak concentration of 20 mM ethanol, GIRK2 puncta in
657 the AF group increased to levels significantly higher than the UN group (Fig. 5B). Similarly,
658 *KCNJ6* mRNA levels were shown to be increased above untreated levels by scRNAseq results
659 (Fig. 1C) as well as FISH analysis (Fig. 5J). Ethanol also increased the proportion of $MAP2^+$ cells
660 expressing *KCNJ6* as well as the expression level per cell (Fig. 5J.b-c). While previous studies
661 identified a binding site for ethanol in a defined pocket of GIRK2[70], suggesting that ethanol
662 could affect protein stabilization, this binding could not explain the increased mRNA level.
663 There is no indication that ethanol or *KCNJ6* haplotype altered translocation of *KCNJ6* mRNA to
664 neuronal processes (Fig. 5J.d-e). Ethanol has been found to affect microRNA expression
665 patterns that regulate mRNA[65, 71-76]. It is intriguing to speculate that ethanol might increase
666 expression of GIRK2 through this type of mechanism, with polymorphisms in the 3'UTR serving
667 as the modulator.

668 **GIRK2 in the context of alcohol dependence**

669 GIRK channels play an essential role in maintaining the excitability of neurons. For example, in
670 Trisomy 21 individuals, whose cells contain an additional copy of *KCNJ6*, neuronal activity was
671 shown to be reduced due to excessive channel activity[77-79]. On the other hand, loss of GIRK2

activity in knockout mice increases susceptibility to induced seizures[20, 21]. We detected the presence of GIRK channel function in glutamatergic iNs using the ML297 agonist of GIRK1/2 heterotetramers, showing that activation led to a reduction in the frequency of action potentials induced by depolarization (Fig. 2D). However, only 6.7% of neurons responded to ML297, but overexpression of GIRK2 increased the proportion of responding neurons to 30% (Fig. 2D). We therefore chose to focus on evaluating neuronal excitability as an indirect response to changes in GIRK function.

By identifying the correlation between GIRK2 expression levels and altered GIRK2-mediated function, we predict that neuronal excitability will be affected by *KCNJ6* variants and alcohol exposure. Human iNs generated from subjects with the variant *KCNJ6* haplotype and AUD were more excitable and had lower levels of GIRK2 expression. Moreover, ethanol exposure, both shorter (1 d) and longer (7 d) term, diminished these differences, mimicking the effect of GIRK2 overexpression. While GIRK channels play relatively small role in maintaining neuronal homeostasis, modulating GIRK activity to alter cell excitability is predicted to play a critical role. Additionally, downstream effectors of the G protein-mediated signaling pathways presumably regulate neuronal function indirectly[14, 15, 17, 19]. GIRK channels are implicated in several other disorders with abnormal neuronal excitability, including epilepsy, suggesting that they have therapeutic potential[19-21, 77-80].

Potential limitations

Several factors beyond *KCNJ6* haplotype may contribute to these interpretations. First, we selected sex-balanced groups because it is possible that the sex of individual neurons might contribute to the results or at least affect variability. However, in nearly all parameters tested, there was no significant difference by sex. The scRNAseq results identified only 6 genes as different by sex and 4 of these are encoded by sex chromosomes. None of the basal morphology measurements (Fig. 3B, D) differed by sex, but membrane capacitance (Fig. 3F.a, $p = 2.6 \times 10^{-4}$), induced APs (step protocol, Fig. 3G.b, $p = 0.012$), and ethanol-treated membrane capacitance (Fig. 5D.a, $p = 3.1 \times 10^{-8}$) all reached significance, but it is difficult to interpret how sex interacts with neuronal function in the context of artificially cultured neurons. Second, the choices we made about pooling subjects for "cell village" experiments (Fig. 1C-E) might have affected results. We chose to mix subjects with the same *KCNJ6* haplotype, fearing a non-cell-autonomous effect based on altered excitability. Finally, we chose to focus on homozygous haplotypes and extreme AUD diagnoses in this study to enhance contrasts, however, additional studies might examine if heterozygotes would exhibit gene dosage effects or be rescued by the presence of the major alleles, similar to endophenotype studies with the original subjects[8].

From genes to behavior

In this study, we found that the variant *KCNJ6* haplotype affects excitability of neurons (Fig. 3 & 4E). In Ca^{2+} imaging experiments, concomitant with enhanced excitability in neurons from affected individuals following stimulation with glutamate pulses, we observed an overall increase in basal activity of the neuronal population (Fig. 4F). This is reminiscent of the original

711 observation linking *KCNJ6* variants with an EEG endophenotype, where Kamarajan and
712 colleagues observed that individuals with alcohol dependence and the *KCNJ6* haplotype had an
713 ERO theta power that varied as a function of the *KCNJ6* haplotype in both loss and gain
714 conditions[10]. There is an extensive human literature linking impulsivity to alcohol use
715 problems[81-84]. Impulsivity is elevated in offspring who are at high risk for substance use
716 disorders and may be a reflection of a genetic vulnerability for substance use problems[85].
717 Excitability in individual neurons and particularly in a culture dish of neurons is several levels of
718 complexity removed from EEG patterns in brain. However, our study points to a mechanistic
719 underpinning of how heritable risk traits are likely to play a role in development of unique
720 physiological response to alcohol in the brain.

721

Acknowledgements

The Collaborative Study on the Genetics of Alcoholism (COGA), Principal Investigators B. Porjesz, V. Hesselbrock, T. Foroud; Scientific Director, A. Agrawal; Translational Director, D. Dick, includes eleven different centers: University of Connecticut (V. Hesselbrock); Indiana University (H.J. Edenberg, T. Foroud, Y. Liu, M. Plawecki); University of Iowa Carver College of Medicine (S. Kuperman, J. Kramer); SUNY Downstate Health Sciences University (B. Porjesz, J. Meyers, C. Kamarajan, A. Pandey); Washington University in St. Louis (L. Bierut, J. Rice, K. Bucholz, A. Agrawal); University of California at San Diego (M. Schuckit); Rutgers University (J. Tischfield, R. Hart, J. Salvatore); The Children's Hospital of Philadelphia, University of Pennsylvania (L. Almasy); Virginia Commonwealth University (D. Dick); Icahn School of Medicine at Mount Sinai (A. Goate, P. Slesinger); and Howard University (D. Scott). Other COGA collaborators include: L. Bauer (University of Connecticut); J. Nurnberger Jr., L. Wetherill, X., Xuei, D. Lai, S. O'Connor, (Indiana University); G. Chan (University of Iowa; University of Connecticut); D.B. Chorlian, J. Zhang, P. Barr, S. Kinreich, G. Pandey (SUNY Downstate); N. Mullins (Icahn School of Medicine at Mount Sinai); A. Anokhin, S. Hartz, E. Johnson, V. McCutcheon, S. Saccone (Washington University); J. Moore, Z. Pang, S. Kuo (Rutgers University); A. Merikangas (The Children's Hospital of Philadelphia and University of Pennsylvania); F. Aliev (Virginia Commonwealth University); H. Chin and A. Parsian are the NIAAA Staff Collaborators. We continue to be inspired by our memories of Henri Begleiter and Theodore Reich, founding PI and Co-PI of COGA, and also owe a debt of gratitude to other past organizers of COGA, including Ting- Kai Li, P. Michael Conneally, Raymond Crowe, and Wendy Reich, for their critical contributions. This national collaborative study is supported by NIH Grant U10AA008401 from the National Institute on Alcohol Abuse and Alcoholism (NIAAA) and the National Institute on Drug abuse (NIDA).

746 ## Conflict of Interest

747 The authors declare no conflict of interest.

748

References

1. Verhulst B, Neale MC, Kendler KS. The heritability of alcohol use disorders: a meta-analysis of twin and adoption studies. *Psychol Med* 2015; **45**(5)**:** 1061-1072.

2. Pollard MS, Tucker JS, Green HD, Jr. Changes in Adult Alcohol Use and Consequences During the COVID-19 Pandemic in the US. *JAMA Network Open* 2020; **3**(9)**:** e2022942-e2022942.

3. Bouza C, Angeles M, Muñoz A, Amate JM. Efficacy and safety of naltrexone and acamprosate in the treatment of alcohol dependence: a systematic review. *Addiction* 2004; **99**(7)**:** 811-828.

4. Heilig M, Egli M. Pharmacological treatment of alcohol dependence: Target symptoms and target mechanisms. *Pharmacology & Therapeutics* 2006; **111**(3)**:** 855-876.

5. Skinner MD, Lahmek P, Pham H, Aubin HJ. Disulfiram efficacy in the treatment of alcohol dependence: a meta-analysis. *PLoS One* 2014; **9**(2)**:** e87366.

6. Salvatore JE, Gottesman, II, Dick DM. Endophenotypes for Alcohol Use Disorder: An Update on the Field. *Curr Addict Rep* 2015; **2**(1)**:** 76-90.

7. Chorlian DB, Rangaswamy M, Manz N, Meyers JL, Kang SJ, Kamarajan C *et al.* Genetic correlates of the development of theta event related oscillations in adolescents and young adults. *Int J Psychophysiol* 2017; **115:** 24-39.

8. Kang SJ, Rangaswamy M, Manz N, Wang JC, Wetherill L, Hinrichs T *et al.* Family-based genome-wide association study of frontal θ oscillations identifies potassium channel gene KCNJ6. *Genes Brain Behav* 2012; **11**(6)**:** 712-719.

9. Clarke TK, Laucht M, Ridinger M, Wodarz N, Rietschel M, Maier W *et al.* KCNJ6 is associated with adult alcohol dependence and involved in gene × early life stress interactions in adolescent alcohol drinking. *Neuropsychopharmacology* 2011; **36**(6)**:** 1142-1148.

10. Kamarajan C, Pandey AK, Chorlian DB, Manz N, Stimus AT, Edenberg HJ *et al.* A KCNJ6 gene polymorphism modulates theta oscillations during reward processing. *Int J Psychophysiol* 2017; **115:** 13-23.

11. Andrew C, Fein G. Event-related oscillations versus event-related potentials in a P300 task as biomarkers for alcoholism. *Alcohol Clin Exp Res* 2010; **34**(4)**:** 669-680.

12. Kamarajan C, Rangaswamy M, Tang Y, Chorlian DB, Pandey AK, Roopesh BN *et al.* Dysfunctional reward processing in male alcoholics: an ERP study during a gambling task. *J Psychiatr Res* 2010; **44**(9)**:** 576-590.

13. Glaaser IW, Slesinger PA. Structural Insights into GIRK Channel Function. *International review of neurobiology* 2015; **123:** 117-160.

14. Luscher C, Slesinger PA. Emerging roles for G protein-gated inwardly rectifying potassium (GIRK) channels in health and disease. *Nat Rev Neurosci* 2010; **11**(5)**:** 301-315.

15. Zhao Y, Gameiro-Ros I, Glaaser IW, Slesinger PA. Advances in Targeting GIRK Channels in Disease. *Trends Pharmacol Sci* 2021; **42**(3)**:** 203-215.

16. Reuveny E, Slesinger PA, Inglese J, Morales JM, Iñiguez-Lluhi JA, Lefkowitz RJ *et al.* Activation of the cloned muscarinic potassium channel by G protein beta gamma subunits. *Nature* 1994; **370**(6485)**:** 143-146.

17. Aryal P, Dvir H, Choe S, Slesinger PA. A discrete alcohol pocket involved in GIRK channel activation. *Nat Neurosci* 2009; **12**(8)**:** 988-995.

18. Bodhinathan K, Slesinger PA. Alcohol modulation of G-protein-gated inwardly rectifying potassium channels: from binding to therapeutics. *Front Physiol* 2014; **5:** 76.

19. Blednov YA, Stoffel M, Chang SR, Harris RA. Potassium channels as targets for ethanol: studies of G-protein-coupled inwardly rectifying potassium channel 2 (GIRK2) null mutant mice. *J Pharmacol Exp Ther* 2001; **298**(2)**:** 521-530.

20. Blednov YA, Stoffel M, Chang SR, Harris RA. GIRK2 deficient mice. Evidence for hyperactivity and reduced anxiety. *Physiol Behav* 2001; **74**(1-2)**:** 109-117.

21. Hill KG, Alva H, Blednov YA, Cunningham CL. Reduced ethanol-induced conditioned taste aversion and conditioned place preference in GIRK2 null mutant mice. *Psychopharmacology (Berl)* 2003; **169**(1)**:** 108-114.

22. Lieberman R, Levine ES, Kranzler HR, Abreu C, Covault J. Pilot study of iPS-derived neural cells to examine biologic effects of alcohol on human neurons in vitro. *Alcohol Clin Exp Res* 2012; **36**(10)**:** 1678-1687.

23. Lieberman R, Kranzler HR, Levine ES, Covault J. Examining the effects of alcohol on GABA(A) receptor mRNA expression and function in neural cultures generated from control and alcohol dependent donor induced pluripotent stem cells. *Alcohol* 2018; **66:** 45-53.

24. Halikere A, Popova D, Scarnati MS, Hamod A, Swerdel MR, Moore JC *et al.* Addiction associated N40D mu-opioid receptor variant modulates synaptic function in human neurons. *Mol Psychiatry* 2020; **25**(7)**:** 1406-1419.

25. Scarnati MS, Boreland AJ, Joel M, Hart RP, Pang ZP. Differential sensitivity of human neurons carrying mu opioid receptor (MOR) N40D variants in response to ethanol. *Alcohol* 2020; **87:** 97-109.

26. Patzke C, Dai J, Brockmann MM, Sun Z, Fenske P, Rosenmund C *et al.* Cannabinoid receptor activation acutely increases synaptic vesicle numbers by activating synapsins in human synapses. *Mol Psychiatry* 2021.

27. Weissbein U, Schachter M, Egli D, Benvenisty N. Analysis of chromosomal aberrations and recombination by allelic bias in RNA-Seq. *Nature communications* 2016; **7:** 12144.

28. Vierbuchen T, Ostermeier A, Pang ZP, Kokubu Y, Sudhof TC, Wernig M. Direct conversion of fibroblasts to functional neurons by defined factors. *Nature* 2010; **463**(7284)**:** 1035-1041.

29. Pang ZP, Yang N, Vierbuchen T, Ostermeier A, Fuentes DR, Yang TQ *et al.* Induction of human neuronal cells by defined transcription factors. *Nature* 2011; **476**(7359)**:** 220-223.

30. Zhang Y, Pak C, Han Y, Ahlenius H, Zhang Z, Chanda S *et al.* Rapid single-step induction of functional neurons from human pluripotent stem cells. *Neuron* 2013; **78**(5)**:** 785-798.

31. Lin HC, He Z, Ebert S, Schörnig M, Santel M, Nikolova MT *et al.* NGN2 induces diverse neuron types from human pluripotency. *Stem Cell Reports* 2021; **16**(9)**:** 2118-2127.

32. Bardy C, van den Hurk M, Eames T, Marchand C, Hernandez RV, Kellogg M *et al.* Neuronal medium that supports basic synaptic functions and activity of human neurons in vitro. *Proc Natl Acad Sci U S A* 2015; **112**(20)**:** E2725-2734.

33. Yang N, Chanda S, Marro S, Ng Y-H, Janas JA, Haag D *et al.* Generation of pure GABAergic neurons by transcription factor programming. *Nature Methods* 2017; **14**(6)**:** 621-628.

34. Kreitzer FR, Salomonis N, Sheehan A, Huang M, Park JS, Spindler MJ *et al.* A robust method to derive functional neural crest cells from human pluripotent stem cells. *Am J Stem Cells* 2013; **2**(2)**:** 119-131.

35. Miyaoka Y, Chan AH, Judge LM, Yoo J, Huang M, Nguyen TD *et al.* Isolation of single-base genome-edited human iPS cells without antibiotic selection. *Nature methods* 2014; **11**(3)**:** 291-293.

36. Ran FA, Hsu PD, Wright J, Agarwala V, Scott DA, Zhang F. Genome engineering using the CRISPR-Cas9 system. *Nature Protocols* 2013; **8**(11)**:** 2281-2308.

37. Chen S, Zhou Y, Chen Y, Gu J. fastp: an ultra-fast all-in-one FASTQ preprocessor. *Bioinformatics (Oxford, England)* 2018; **34**(17)**:** i884-i890.

38. Kim D, Paggi JM, Park C, Bennett C, Salzberg SL. Graph-based genome alignment and genotyping with HISAT2 and HISAT-genotype. *Nature Biotechnology* 2019; **37**(8)**:** 907-915.

39. Danecek P, Bonfield JK, Liddle J, Marshall J, Ohan V, Pollard MO *et al.* Twelve years of SAMtools and BCFtools. *GigaScience* 2021; **10**(2).

40. McLaren W, Gil L, Hunt SE, Riat HS, Ritchie GRS, Thormann A *et al.* The Ensembl Variant Effect Predictor. *Genome Biology* 2016; **17**(1)**:** 122.

41. Butler A, Hoffman P, Smibert P, Papalexi E, Satija R. Integrating single-cell transcriptomic data across different conditions, technologies, and species. *Nat Biotechnol* 2018; **36**(5)**:** 411-420.

42. Kang HM, Subramaniam M, Targ S, Nguyen M, Maliskova L, McCarthy E *et al.* Multiplexed droplet single-cell RNA-sequencing using natural genetic variation. *Nat Biotechnol* 2018; **36**(1)**:** 89-94.

43. Love MI, Huber W, Anders S. Moderated estimation of fold change and dispersion for RNA-seq data with DESeq2. *Genome Biol* 2014; **15**(12)**:** 550.

44. Wu T, Hu E, Xu S, Chen M, Guo P, Dai Z *et al.* clusterProfiler 4.0: A universal enrichment tool for interpreting omics data. *Innovation (N Y)* 2021; **2**(3)**:** 100141.

45. Schneider CA, Rasband WS, Eliceiri KW. NIH Image to ImageJ: 25 years of image analysis. *Nature methods* 2012; **9**(7)**:** 671-675.

46. Ho S-Y, Chao C-Y, Huang H-L, Chiu T-W, Charoenkwan P, Hwang E. NeurphologyJ: An automatic neuronal morphology quantification method and its application in pharmacological discovery. *BMC Bioinformatics* 2011; **12**(1)**:** 230.

47. Arganda-Carreras I, Kaynig V, Rueden C, Eliceiri KW, Schindelin J, Cardona A *et al.* Trainable Weka Segmentation: a machine learning tool for microscopy pixel classification. *Bioinformatics* 2017; **33**(15)**:** 2424-2426.

48. Fantuzzo JA, Robles DA, Mirabella VR, Hart RP, Pang ZP, Zahn JD. Development of a high-throughput arrayed neural circuitry platform using human induced neurons for drug screening applications. *Lab Chip* 2020; **20**(6)**:** 1140-1152.

49. Zhang ZM, Chen S, Liang YZ. Baseline correction using adaptive iteratively reweighted penalized least squares. *Analyst* 2010; **135**(5)**:** 1138-1146.

50. Bates D, Mächler M, Bolker B, Walker S. Fitting Linear Mixed-Effects Models Using lme4. *Journal of Statistical Software* 2015; **67**(1)**:** 1 - 48.

51. Højsgaard S, Halekoh U, Yan J. The R Package geepack for Generalized Estimating Equations. *Journal of Statistical Software* 2005; **15**(2)**:** 1 - 11.

52. Mitchell JM, Nemesh J, Ghosh S, Handsaker RE, Mello CJ, Meyer D *et al.* Mapping genetic effects on cellular phenotypes with “cell villages”. *bioRxiv* 2020**:** 2020.2006.2029.174383.

53. Lesage F, Guillemare E, Fink M, Duprat F, Heurteaux C, Fosset M *et al.* Molecular properties of neuronal G-protein-activated inwardly rectifying K+ channels. *J Biol Chem* 1995; **270**(48)**:** 28660-28667.

54. Ang CE, Wernig M. Induced neuronal reprogramming. *J Comp Neurol* 2014; **522**(12)**:** 2877-2886.

55. Shelby H, Shelby T, Wernig M. Somatic Lineage Reprogramming. *Cold Spring Harb Perspect Biol* 2021.

56. Marron Fernandez de Velasco E, Zhang L, B NV, Tipps M, Farris S, Xia Z *et al.* GIRK2 splice variants and neuronal G protein-gated K(+) channels: implications for channel function and behavior. *Sci Rep* 2017; **7**(1)**:** 1639.

57. Cáceres A, Banker GA, Binder L. Immunocytochemical localization of tubulin and microtubule-associated protein 2 during the development of hippocampal neurons in culture. *J Neurosci* 1986; **6**(3)**:** 714-722.

58. Ma F, Xu J, Liu Y, Popova D, Youssef MM, Hart RP *et al.* The amyloid precursor protein modulates the position and length of the axon initial segment offering a new perspective on Alzheimer’s disease genetics. *bioRxiv* 2022**:** 2022.2001.2023.477413.

59. Wydeven N, Marron Fernandez de Velasco E, Du Y, Benneyworth MA, Hearing MC, Fischer RA *et al.* Mechanisms underlying the activation of G-protein-gated inwardly rectifying K+ (GIRK) channels by the novel anxiolytic drug, ML297. *Proc Natl Acad Sci U S A* 2014; **111**(29)**:** 10755-10760.

60. Days E, Kaufmann K, Romaine I, Niswender C, Lewis M, Utley T *et al.* Discovery and Characterization of a Selective Activator of the G-Protein Activated Inward-Rectifying Potassium (GIRK) Channel. *Probe Reports from the NIH Molecular Libraries Program*. National Center for Biotechnology Information (US): Bethesda (MD), 2010.

61. Kang S, Chen X, Gong S, Yu P, Yau S, Su Z *et al.* Characteristic analyses of a neural differentiation model from iPSC-derived neuron according to morphology, physiology, and global gene expression pattern. *Scientific reports* 2017; **7**(1)**:** 12233.

62. Chen TW, Wardill TJ, Sun Y, Pulver SR, Renninger SL, Baohan A *et al.* Ultrasensitive fluorescent proteins for imaging neuronal activity. *Nature* 2013; **499**(7458)**:** 295-300.

63. Steri M, Idda ML, Whalen MB, Orrù V. Genetic variants in mRNA untranslated regions. *Wiley Interdiscip Rev RNA* 2018; **9**(4)**:** e1474.

64. Wang D, Liu S, Warrell J, Won H, Shi X, Navarro FCP *et al.* Comprehensive functional genomic resource and integrative model for the human brain. *Science* 2018; **362**(6420).

65. Nunez YO, Mayfield RD. Understanding Alcoholism Through microRNA Signatures in Brains of Human Alcoholics. *Front Genet* 2012; **3:** 43.

66. Wehrspaun C, Ponting C, Marques A. Brain-expressed 3′UTR extensions strengthen miRNA cross-talk between ion channel/transporter encoding mRNAs. *Frontiers in Genetics* 2014; **5**(41).

67. Suda S, Nibuya M, Suda H, Takamatsu K, Miyazaki T, Nomura S *et al.* Potassium channel mRNAs with AU-rich elements and brain-specific expression. *Biochem Biophys Res Commun* 2002; **291**(5)**:** 1265-1271.

68. Sun JW, D.; Wong, G.; Lau, T.-M.; Yang, M.; Hart, R.P.; Kwan, K.-M.; Chan, H.Y.E.; Chow, K.H. Chronic alcohol metabolism results in DNA repair infidelity and cell-cycle-induced senescence in neurons. Submitted 2022.

69. Brenner E, Tiwari GR, Kapoor M, Liu Y, Brock A, Mayfield RD. Single cell transcriptome profiling of the human alcohol-dependent brain. *Hum Mol Genet* 2020; **29**(7)**:** 1144-1153.

70. Bodhinathan K, Slesinger PA. Molecular mechanism underlying ethanol activation of G-protein-gated inwardly rectifying potassium channels. *Proc Natl Acad Sci U S A* 2013; **110**(45)**:** 18309-18314.

71. Sathyan P, Golden HB, Miranda RC. Competing interactions between micro-RNAs determine neural progenitor survival and proliferation after ethanol exposure: evidence from an ex vivo model of the fetal cerebral cortical neuroepithelium. *J Neurosci* 2007; **27**(32)**:** 8546-8557.

72. Pietrzykowski AZ, Friesen RM, Martin GE, Puig SI, Nowak CL, Wynne PM *et al.* Posttranscriptional regulation of BK channel splice variant stability by miR-9 underlies neuroadaptation to alcohol. *Neuron* 2008; **59**(2)**:** 274-287.

73. Lewohl JM, Nunez YO, Dodd PR, Tiwari GR, Harris RA, Mayfield RD. Up-regulation of microRNAs in brain of human alcoholics. *Alcohol Clin Exp Res* 2011; **35**(11)**:** 1928-1937.

74. Osterndorff-Kahanek EA, Tiwari GR, Lopez MF, Becker HC, Harris RA, Mayfield RD. Long-term ethanol exposure: Temporal pattern of microRNA expression and associated mRNA gene networks in mouse brain. *PLoS One* 2018; **13**(1)**:** e0190841.

75. Lim Y, Beane-Ebel JE, Tanaka Y, Ning B, Husted CR, Henderson DC *et al.* Exploration of alcohol use disorder-associated brain miRNA-mRNA regulatory networks. *Translational psychiatry* 2021; **11**(1)**:** 504.

76. Zhu S, Wu J, Hu J. Non-coding RNA in alcohol use disorder by affecting synaptic plasticity. *Exp Brain Res* 2022.

77. Best TK, Siarey RJ, Galdzicki Z. Ts65Dn, a mouse model of Down syndrome, exhibits increased GABAB-induced potassium current. *J Neurophysiol* 2007; **97**(1)**:** 892-900.

78. Harashima C, Jacobowitz DM, Witta J, Borke RC, Best TK, Siarey RJ *et al.* Abnormal expression of the G-protein-activated inwardly rectifying potassium channel 2 (GIRK2) in hippocampus, frontal cortex, and substantia nigra of Ts65Dn mouse: a model of Down syndrome. *J Comp Neurol* 2006; **494**(5)**:** 815-833.

79. Reeves RH, Irving NG, Moran TH, Wohn A, Kitt C, Sisodia SS *et al.* A mouse model for Down syndrome exhibits learning and behaviour deficits. *Nat Genet* 1995; **11**(2)**:** 177-184.

80. Kleschevnikov AM, Yu J, Kim J, Lysenko LV, Zeng Z, Yu YE *et al.* Evidence that increased Kcnj6 gene dose is necessary for deficits in behavior and dentate gyrus synaptic plasticity in the Ts65Dn mouse model of Down syndrome. *Neurobiol Dis* 2017; **103:** 1-10.

81. Congdon E, Canli T. The endophenotype of impulsivity: reaching consilience through behavioral, genetic, and neuroimaging approaches. *Behav Cogn Neurosci Rev* 2005; **4**(4)**:** 262-281.

82. Dick DM, Smith G, Olausson P, Mitchell SH, Leeman RF, O'Malley SS *et al.* Understanding the construct of impulsivity and its relationship to alcohol use disorders. *Addict Biol* 2010; **15**(2)**:** 217-226.

83. Sher KJ, Trull TJ. Personality and disinhibitory psychopathology: alcoholism and antisocial personality disorder. *J Abnorm Psychol* 1994; **103**(1)**:** 92-102.

84. Verdejo-García A, Lawrence AJ, Clark L. Impulsivity as a vulnerability marker for substance-use disorders: review of findings from high-risk research, problem gamblers and genetic association studies. *Neurosci Biobehav Rev* 2008; **32**(4)**:** 777-810.

85. Polich J, Bloom FE. P300, alcoholism heritability, and stimulus modality. *Alcohol* 1999; **17**(2)**:** 149-156.

1064 # Figure Legends

1065 **Figure 1. Experimental design and gene expression analysis**
1066 **A.** Diagram outlining experimental design. Lymphocytes from subjects with or without AUD
1067 diagnosis and *KCNJ6* haplotype variants were selected, reprogrammed into iPSC, induced into
1068 excitatory iNs, and analyzed by morphometry, immunocytochemistry, gene expression, and
1069 electrophysiology. **B.** Sequencing alignment and depth analysis of bulk RNA sequencing
1070 confirmed expression of *KCNJ6* mRNA in iN cultures, specifically the ENST00000609713 isoform,
1071 containing an 18.1 kilobase 3'UTR region. *KCNJ6* exons are mapped to chromosome locations
1072 (marked in mb, megabases) and the position of the gene is indicated by the red box on the
1073 chromosome 21 pictogram, top, with transcription direction on the minus strand indicated by
1074 the broken arrow. Variant analysis of RNA sequences predicts a region of linkage disequilibrium
1075 of 22 SNPs, including the 3 SNPs used to select subjects (red, Table 1), and 19 additional SNPs
1076 (blue, Supplemental Table 1). Depth: number of sequencing reads per base aligned by position.
1077 Frequency: thickness of curved lines represents the relative frequency of splice site utilization
1078 between exons. **C.** Single-cell RNAseq identifies a cluster of induced neurons (lower left),
1079 expressing markers consistent with neuronal function including *SYP*, *SLC17A6*, *GRIN2B*, *SCN3A*,
1080 *KCNJ3*, and *KCNJ6*; distinct from "transition neurons" that either do not express these markers
1081 or express sporadically. Additional markers are plotted in Supplemental Fig. 2E. Isolating *KCNJ6*
1082 mRNA expression, aggregated by subject and treatment, AF neurons expressed a trend towards
1083 lower levels than UN neurons ($p = 0.0508$; Wald test), but treatment of 7d with IEE at 20 mM
1084 peak concentration increased AF expression above untreated ($p = 0.0225$) to levels similar to
1085 UN control ($p = 0.322$, not denoted on figure). **D.** Volcano plot for untreated UN vs AF neurons,
1086 highlighting genes significantly different (FDR > 0.05) and at least 1.5-fold changed (red dots).
1087 Genes below the fold-change cut-off are marked in green, and those not significantly different
1088 are marked in blue. Significantly different genes are listed in Supplemental Table 3. **F.** Gene
1089 ontology (GO) enrichment of top 10 biological process (BP) terms for up- or down-regulated
1090 genes. Plots indicate the number of regulated genes from the term and the color indicates the
1091 adjusted p-value (q-value; key). All enriched terms are listed in Supplemental Tables 4-5.

1092 **Figure 2. Validation of GIRK2 expression and function in human induced neurons.**
1093 **A**. Representative confocal images of GIRK2 immunoreactivity in mouse cortical neurons.
1094 Arrowheads indicate locations of GIRK2-staining puncta, with an example punctum enlarged in
1095 the inset, overlapping or adjacent to βIII-tubulin-positive processes. We observed two cellular
1096 expression patterns – one where the entire neuron is decorated with GIRK2 antibody
1097 (Supplemental Fig. 4), or another where GIRK2 expression is relatively faint and observed
1098 mostly on neuronal processes, shown here. **B**. GIRK2 expression patterns in human induced
1099 neurons (iNs), showing representative confocal images from line 420. Inset shows two adjacent
1100 puncta. **C**. Following infection of iN cultures with lentivirus expressing both *KCNJ6* and mCherry,
1101 large numbers of $GIRK2^+$ puncta are seen in representative images (line 420). **D**. Evaluation of
1102 GIRK2 function in iNs, (a) quantification of GIRK2 expression on $MAP2^+$ vs. βIII-$tubulin^+$ neuronal

1103 processes. GIRK2 is more abundant on βIII-tubulin processes (p=0.0006, one-tailed Student's t-
1104 test, n=15 cells per group, cell line 420). (b) Basal levels (upper pie plot) of the GIRK current in
1105 iNs as percent of neurons responding with hyperpolarization to the selective GIRK activator
1106 (160 nM ML297); compared with responding percentage when GIRK2 is overexpressed (lower
1107 pie chart). (c) Representative image of iN overexpressing GIRK2, as confirmed with mCherry
1108 fluorescence. (d) Representative traces of induced action potential firing before and after GIRK
1109 activation, demonstrating the contribution of GIRK function to cell excitability. (e)
1110 Representative trace of spontaneous postsynaptic potential (sEPSCs) recordings during ML297
1111 (160 nM) GIRK activator wash-in, demonstrating a shift of 7mV holding current (amplifier-
1112 dependent compensation of GIRK-mediated membrane hyperpolarization). (f) Quantification of
1113 neuronal excitability at baseline and following GIRK activation with 160 nM ML297 (p=0.015,
1114 paired Student's t-test, n=9 cells before/after ML297, cell line 376).

1115 **Figure 3. Impact of AUD-associated *KCNJ6* haplotype on neuronal properties.**
1116 **A**. Principles of morphological analysis of induced neurons: (a) Neurite area was the total TuJ1$^+$
1117 (βIII-tubulin)$^+$ staining area outside the cell soma. (b) Solidity is the area of the soma divided by
1118 its convex hull area. (c) Soma size was the area of the MAP2$^+$ cell body. (d) Circularity compared
1119 the perimeter to the area. **B**. Morphometry of iNs from *KCNJ6* haplotype variant and affected
1120 (**AF**, cyan) or unaffected (**UN**, grey) individuals. Results are summed by group (left) or plotted
1121 individually by cell line (right), with subjects identified by line number (see Table 1—females
1122 identified with grey numbers). Individual cells are plotted as dots with the bar showing the
1123 mean, with error bars indicating the standard error of the mean (SEM). No significant
1124 differences were found in (a) soma size, (b) circularity, or (c) soma solidity, but total neurite
1125 area was increased in the AF group (p =0.018). **C**. Representative images of iNs from individual
1126 lines, with arrows identifying individual GIRK2 puncta (red) localized on βIII-tubulin$^+$ processes
1127 (gray). **D**. GIRK2 expression was decreased in the AF as measured by puncta counts (a, p =
1128 0.0012), circularity (c, p = 0.007), or solidity (d, p = 0.037), while there was no difference in
1129 puncta size (b). **E**. Representative images of individual GIRK2 puncta (red) localized on βIII-
1130 tubulin$^+$ processes (gray). **F**. Electrophysiological analysis of passive neuronal properties,
1131 showing no difference in (a) membrane capacitance (b) membrane resistance, or (c)
1132 spontaneous EPSCs frequency. (d) Representative sEPSCs traces for each line. (e) Spontaneous
1133 EPSCs amplitude. **G**. Electrophysiological analysis of active neuronal properties. (a)
1134 Quantification of current required to shift resting membrane potential to -65mV in pA:
1135 difference by group p = 1.2 x 10^{-5}; (b) quantification of maximum number of action potentials
1136 (APs) induced with the "step" protocol, p = 0.086; (c) representative traces of APs induced with
1137 the "step" protocol; (d) quantification of number of action potentials (APs) induced with the
1138 "ramp" protocol, p = 2.0 x 10^{-9}; (e) representative traces of APs induced with the "ramp"
1139 protocol. A generalized linear model was used to evaluate group differences for morphometry
1140 and GIRK2 expression, and generalized estimation equations was used for electrophysiology
1141 results. Numbers of cell lines and replicates for each experiment are shown in Supplemental
1142 Table 6.

1143 **Figure 4. Evaluation of neuronal excitability in human induced neuron populations.**
1144 **A.** Representative epifluorescence images of GcaMP6f expression in iNs from affected (233,
1145 246) and unaffected individuals (420, 472). **B, C.** Raster plots of the calcium spiking pattern of
1146 representative experiments from unaffected neurons (**B**, individual 472) and affected neurons
1147 (**C**, individual 233), under the stimulation protocol used. Green and purple bars show the
1148 application of 30 s pulses of Glu 10-50 µM and KCl 18 mM, respectively, on the neuron
1149 populations during the stimulation protocol. Arrows show the epochs of the calcium imaging
1150 recordings selected for calcium spike quantification: baseline, glutamate pulse 1, and KCl pulse
1151 1. **D.** Stimulation protocol (upper bar) and representative raw fluorescence trace (AF individual
1152 233) from a complete recording. The zoom-ins on the first glutamate and KCl pulses depict
1153 glutamate and KCl elicited activity, respectively. The vertical dotted lines correspond to the
1154 calcium spikes detected after analysis. **E, F, G.** Number of spikes per ROI per minute during
1155 baseline (**E**, spontaneous activity), glutamate pulse 1 (**F**, glutamate-elicited activity) and KCl
1156 pulse 1 (**G**, KCl-elicited activity). The pie charts represent the proportion of neurons of UN (grey)
1157 and AF (blue) individuals that exhibited a certain number of calcium spikes during each three
1158 epochs of the recording. The bar plots show the number of spikes per ROI per minute fired by
1159 unaffected individuals (grey) and affected individuals (blue) during baseline, glutamate pulse 1
1160 and KCl pulse 1. The sample size is depicted in the bar of each group as number of iN
1161 batches/number of experiments/number of neurons. Differences between affected and unaffected
1162 groups were evaluated by two-tailed unpaired Student's t-test (Welch's correction for non-equal SD, **p
1163 < 0.01, ****p < 0.0001).

1164 **Figure 5. Ethanol treatment reduced *KCNJ6* haplotype differences in iN excitability and GIRK2**
1165 **expression.**
1166 **A**. Morphological analysis of IEE iNs generated from affected and unaffected individuals,
1167 showing no difference in: (a) neuronal soma size (p = 0.32); (b) soma circularity (p = 0.54); (c)
1168 soma solidity (p = 0.92); and (d) total neurite area (p = 0.98). **B**. There was no difference in
1169 GIRK2 expression in the IEE AF group iNs compared with UN by (a) puncta counts (p = 0.46), (b)
1170 puncta size (p = 0.36), (c) puncta circularity (p = 0.052), or (d) solidity (p = 0.47). **C**.
1171 Representative images of individual GIRK2 puncta (red) localized on βIII-Tubulin positive
1172 processes (gray) for each cell line. **D**. Electrophysiological analysis of passive neuronal
1173 properties in IEE iNs, showing (a) a small decrease in AF membrane capacitance ($p = 9.6 \times 10^{-9}$),
1174 but no difference in (b) membrane resistance (p = 0.63), (c) spontaneous EPSCs frequency (p =
1175 0.32), or (d) spontaneous EPSCs amplitude (p = 0.19). (e) Representative sEPSCs traces for each
1176 cell line. (f) The AF group exhibited no change in resting membrane potential after IEE (p =
1177 0.79). **E**. Electrophysiological analysis of active neuronal properties found no difference in IEE
1178 iNs for (a) current required to shift resting membrane potential to -65mV (p = 0.32), (b)
1179 maximum number of action potentials (APs) induced with the "step" protocol (p = 0.48), with
1180 (c) representative traces of APs induced with the "step" protocol, (d) number of action
1181 potentials (APs) induced with the "ramp" protocol (p = 0.95), with (e) representative traces of
1182 APs induced with the "ramp" protocol. **F**. Representative images from individual lines of iNs,

1183 exposed to 7d of IEE, marked with arrows pointing to individual GIRK2 puncta (red) localized on
1184 βIII-Tubulin positive processes (gray). **G**. Summarized results from all lines showing differences
1185 in GIRK2 expression levels before and after 7 days of 20 mM IEE with ethanol (EtOH; $p = 1.0 \times$
1186 10^{-20}). **H.** Representative images of individual GIRK2 puncta (red) localized on βIII-Tubulin
1187 positive processes (gray) prior and following 7 days 20 mM IEE with ethanol. Sample images are
1188 from line 246. **I.** Representative images of FISH detection of *KCNJ6* mRNA for each cell line. **J.**
1189 Quantification of FISH. (a) The number of *KCNJ6* puncta normalized to the number of cells in an
1190 image shows decreased expression in control AF compared with UN ($p = 8.2 \times 10^{-3}$), increased
1191 expression following IEE ($p = 8.2 \times 10^{-3}$; using Tukey's pairwise comparisons). (b) The percentage
1192 of *KCNJ6*-expressing $MAP2^{+}$ cells substantially increase in the (c) AF group but not in the (b) UN
1193 group. Numbers of *KCNJ6* puncta were analyzed by expression levels per cell, as recommended
1194 by the FISH manufacturer in (d) UN or (e) AF cells. (f) *KCNJ6* puncta within the neuronal soma
1195 show increases following IEE in both UN and AF groups ($p = 0.006$ for genotype, Tukey's post-
1196 hoc for UN, $p = 0.01$, for AF, $p = 0.01$). (g) A similar analysis of non-somatic puncta, presumably
1197 within neurites, showed no differences following IEE between genotypes ($p=0.23$).

1198 **Figure 6. GIRK2 overexpression mimics ethanol response**
1199 **A.** Current required to shift resting membrane potential to -65mV, in untreated (control, $p = 5.9$
1200 $\times 10^{-4}$), lentiviral *KCNJ6* overexpression (over., $p = 0.23$), or 1 d 20 mM IEE (EtOH, $p = 0.75$)
1201 cultures. **B.** Representative traces of APs induced with the "ramp" protocol. **C.** Quantification of
1202 maximum number of action potentials (APs) induced with "ramp" protocol, control ($p = 6.8 \times$
1203 10^{-6}), overexpression ($p = 0.014$), or 1 d 20 mM IEE ($p = 0.10$). **D.** quantification of GIRK2 puncta
1204 after overexpression (line 376, one-tailed Student's t-test $p = 0.04$).

1205

1206 # Supplementary Materials

1207 **Supplemental Tables 1-6:** https://doi.org/10.6084/m9.figshare.19798882.v2

1208 **Supplemental Table 1. SNPs identified in RNAseq samples.** Variants were identified in the
1209 region surrounding KCNJ6 (chr21: 37499112-38245792) using samtools mpileup to bcftools call,
1210 followed by filtering to remove low quality. Results were loaded into the Ensembl VEP tool. A
1211 dot (".") indicates missing data and/or low quality. The reference allele and alternate alleles
1212 were obtained from the UCSC Genome Table Browser.

1213 **Supplemental Table 2: CellRanger parameters for scRNAseq libraries.** Output from CellRanger
1214 shows the alignment statistics and numbers of reads confidently mapped.

1215 **Supplemental Table 3. Differentially expressed genes (DEG) comparing AF to UN without**
1216 **exposure to ethanol.** The table contains all output from DESeq2 results. Excel filters are set to
1217 show only genes significantly different (padj <= 0.05) and at least 1.5-fold different
1218 (abs(log2FoldChange) > 0.585). Release the filters to see the full list.

1219 **Supplemental Table 4. Enriched Gene Ontology-Biological Process (GO-BP) terms from genes**
1220 **increased in AF relative to UN.**

1221 **Supplemental Table 5. Enriched Gene Ontology-Biological Process (GO-BP) terms from genes**
1222 **decreased in AF relative to UN.**

1223 **Supplemental Table 6. Numbers of replicates.** For each parameter tested with statistics, the
1224 numbers of cells and/or microscope fields is indicated and labeled by Figure numbers/letters.

1225 **Supplemental Figures:** https://doi.org/10.6084/m9.figshare.19798873.v3

1226

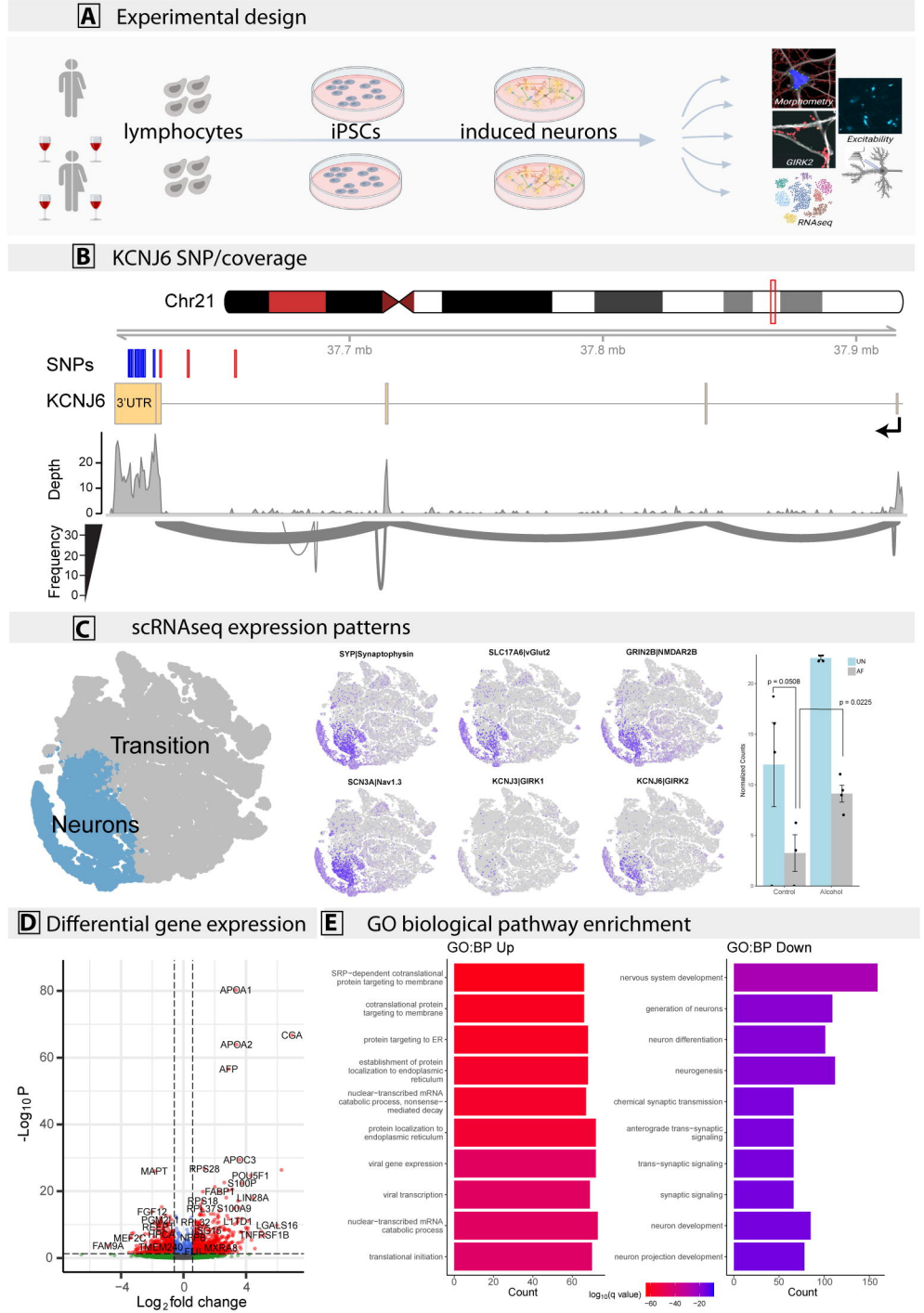

Figure 1, Popova et al., 2022

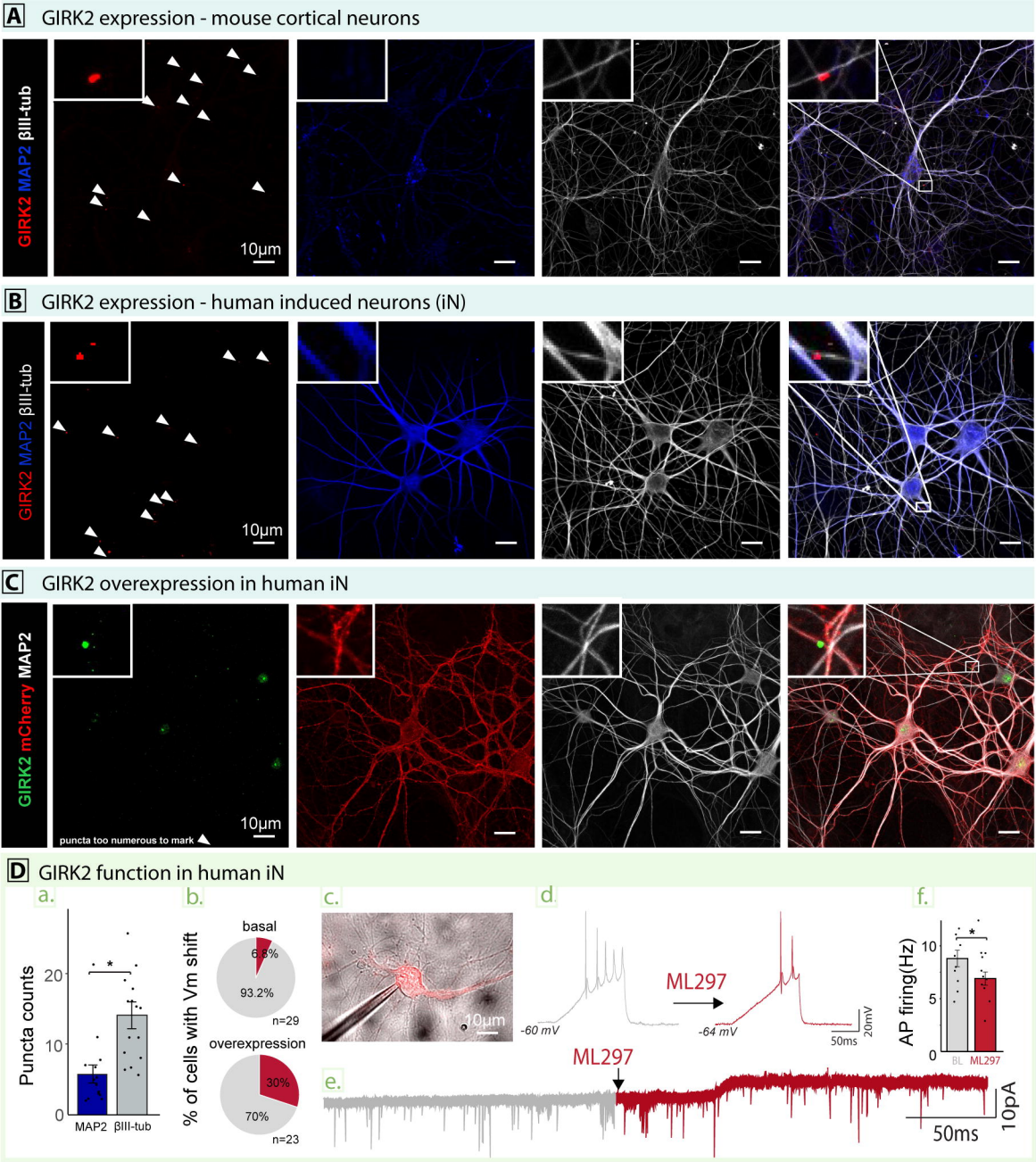

Figure 2, Popova et al., 2022

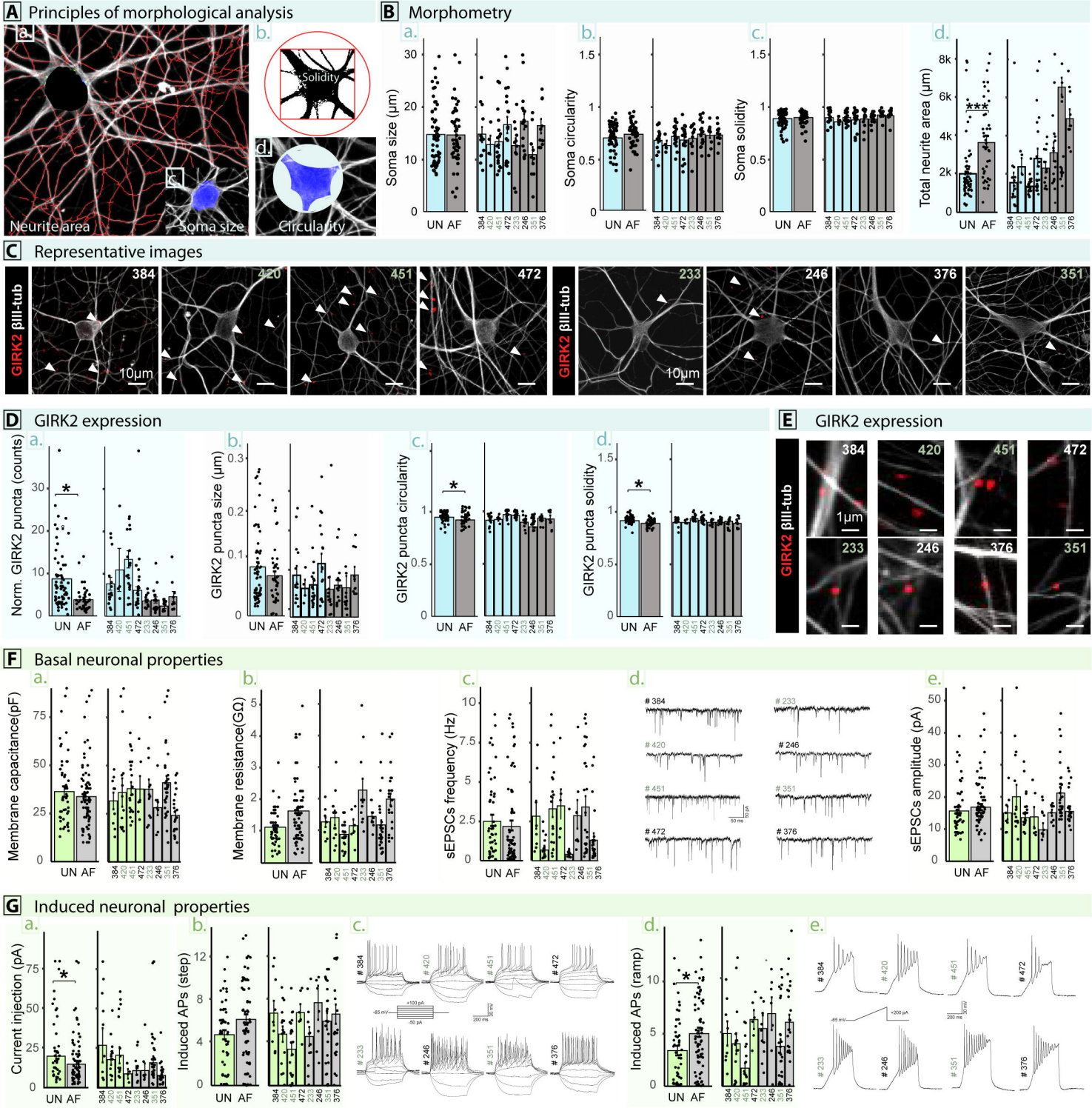

Figure 3, Popova et al., 2022

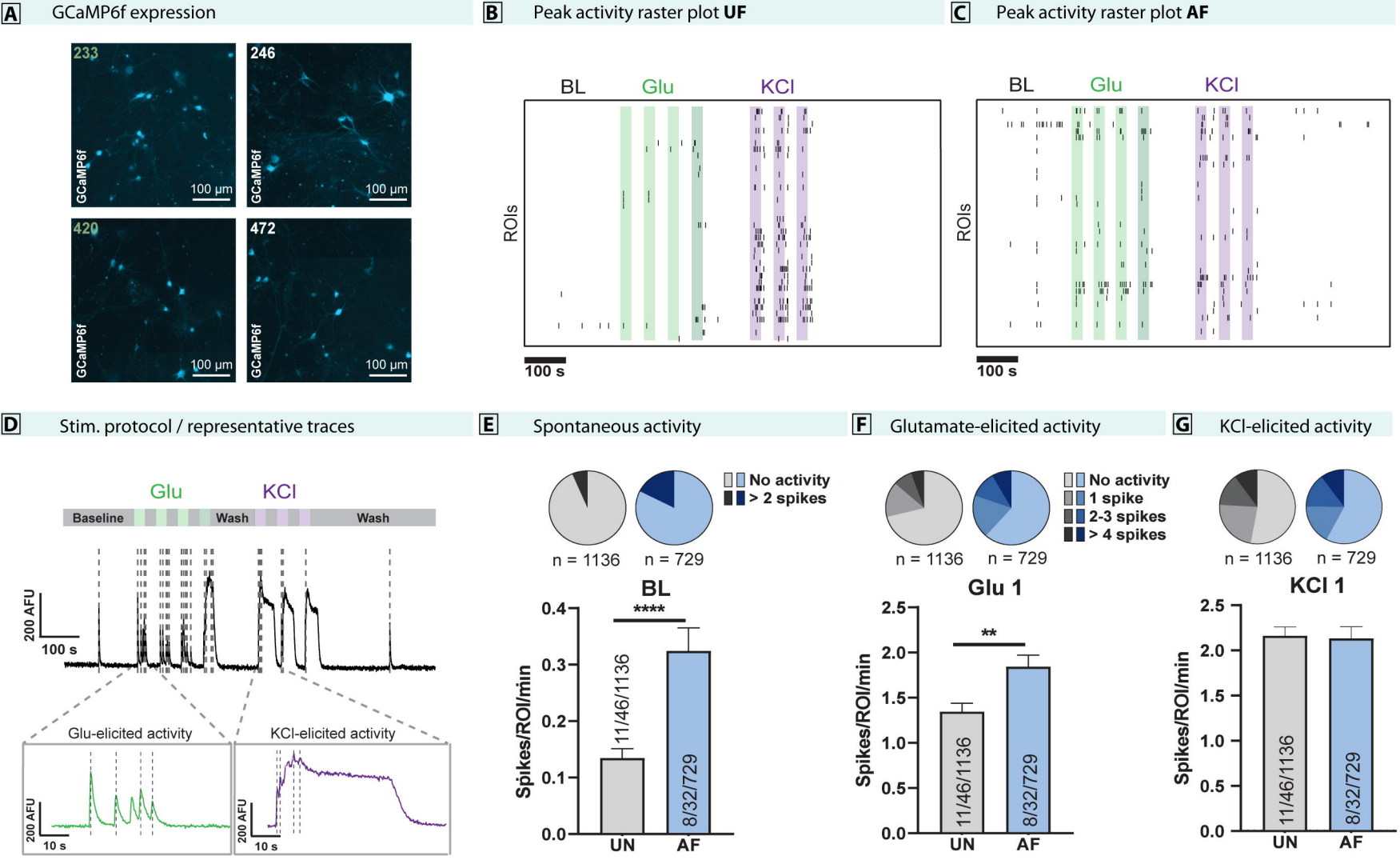

Figure 4, Popova et al., 2022

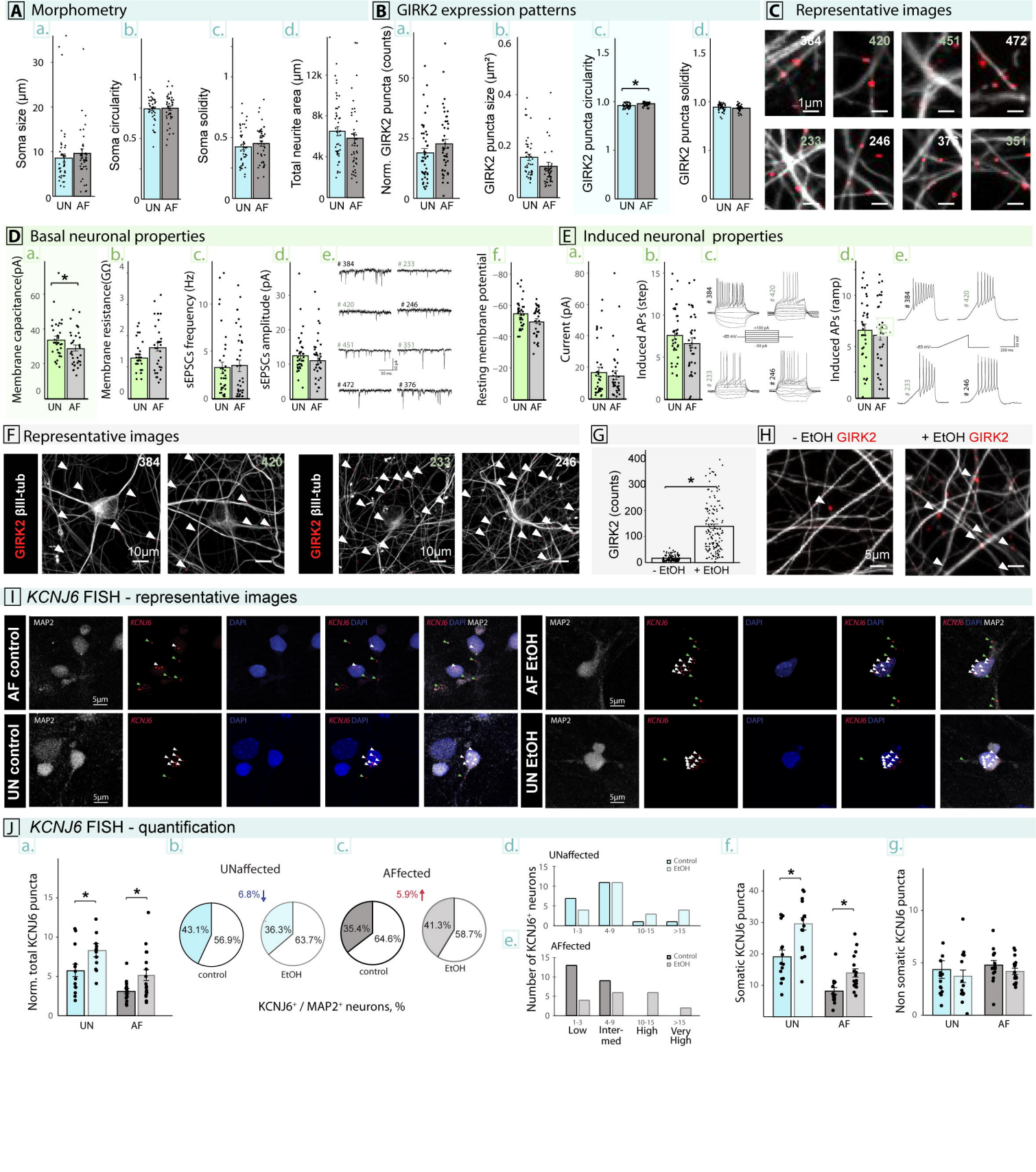

Figure 5, Popova et al., 2022

Active neuronal properties

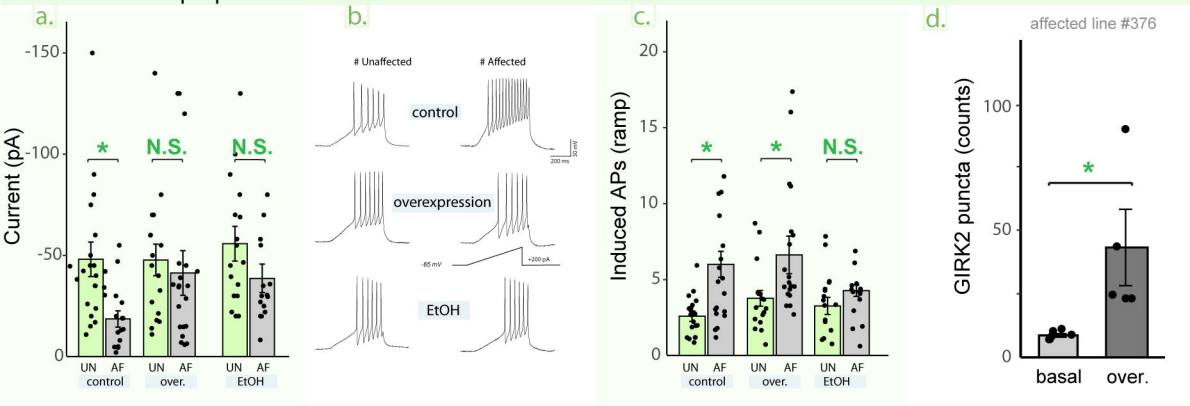

Figure 6, Popova et al., 2022